J|A|C|S
ARTICLES
Published on Web 06/14/2006

Chemistry of Mangana- and Rhenatricarbadecaboranyl Tricarbonyl Complexes: Evidence for an Associative Mechanism of Ligand Substitution Involving an $\eta^6-\eta^4$ Cage-Slippage Process Analagous to $\eta^5-\eta^3$-Cyclopentadienyl Ring-Slippage

Robert Butterick III, Bhaskar M. Ramachandran, Patrick J. Carroll, and Larry G. Sneddon*

Contribution from the Department of Chemistry, University of Pennsylvania, Philadelphia, Pennsylvania 19104-6323

Received April 7, 2006; E-mail: lsneddon@sas.upenn.edu

Abstract: The reaction of the tricarbadecaboranyl anion, 6-Ph-*nido*-5,6,9-$C_3B_7H_9^-$, with $M(CO)_5Br$ [M = Mn, Re] or $[(\eta^6\text{-}C_{10}H_8)Mn(CO)_3^+]BF_4^-$ yielded the half-sandwich metallatricarbadecaboranyl analogues of $(\eta^5\text{-}C_5H_5)M(CO)_3$ [M = Mn, Re]. For both 1,1,1-$(CO)_3$-2-Ph-*closo*-1,2,3,4-$MC_3B_7H_9$ [M = Mn (**2**) and Re (**3**)], the metal is η^6-coordinated to the puckered six-membered open face of the tricarbadecaboranyl cage. Reactions of **2** and **3** with isocyanide at room temperature produced complexes 8-($CNBu^t$)-8,8,8-$(CO)_3$-9-Ph-*nido*-8,7,9,10-$MC_3B_7H_9$ [M = Mn (**4**), Re (**5**)], having the cage η^4-coordinated to the metal. Photolysis of **4** and **5** then resulted in the loss of CO and the formation of 1-($CNBu^t$)-1,1-$(CO)_2$-2-Ph-*closo*-1,2,3,4-$MC_3B_7H_9$ [M = Mn, Re (**6**)], where the cage is again η^6-coordinated to the metal. Reaction of **2** and **3** with 1 equiv of phosphine at room temperature produced the η^6-coordinated monosubstituted complexes 1,1-$(CO)_2$-1-$P(CH_3)_3$-2-Ph-*closo*-1,2,3,4-$MC_3B_7H_9$ [M = Mn (**7**), Re (**9**)] and 1,1-$(CO)_2$-1-$P(C_6H_5)_3$-2-Ph-*closo*-1,2,3,4-$MC_3B_7H_9$ [M = Mn (**8**), Re (**10**)]. NMR studies of these reactions at −40 °C showed that substitution occurs by an associative mechanism involving the initial formation of intermediates having structures similar to those of the η^4-complexes **4** and **5**. The observed $\eta^6-\eta^4$ cage-slippage is analogous to the $\eta^5-\eta^3$ ring-slippage that has been proposed to take place in related substitution reactions of cyclopentadienyl−metal complexes. Reaction of **9** with an additional equivalent of $P(CH_3)_3$ gave 8,8-$(CO)_2$-8,8-$(P(CH_3)_3)_2$-9-Ph-*nido*-8,7,9,10-$ReC_3B_7H_9$ (**11**), where the cage is η^4-coordinated to the metal. Photolysis of **11** resulted in the loss of CO and the formation of the disubstituted η^6-complex 1-CO-1,1-$(P(CH_3)_3)_2$-2-Ph-*closo*-1,2,3,4-$ReC_3B_7H_9$ (**12**).

Introduction

We have previously shown that, although the coordination properties[1] of the tricarbadecaboranyl ligand, 6-R-*nido*-5,6,9-$C_3B_7H_9^-$ [R = Me,[2] Ph[1h]], are in many ways similar to those of the cyclopentadienide monoanion (Figure 1), the metallatricarbadecaboranyl complexes have increased oxidative, chemical, thermal, and hydrolytic stabilities compared to their metallocene counterparts. For example, the vanadatricarbadecaboranyl complexes $(Me\text{-}C_3B_7H_9)_2V$ are air- and moisture-stable,[1g] whereas the corresponding vanadocene $(\eta^5\text{-}C_5H_5)_2V$ is not. We have also recently reported[1i,j] that the tricarbadecaboranyl ligand is capable of undergoing an $\eta^6-\eta^4$ cage-slippage process, with a concomitant decrease in its electron donation to the metal from six to four electrons, that is analogous to that of the $\eta^5-\eta^3$ ring-slippage processes which has been proposed to occur in the associative substitution reactions of

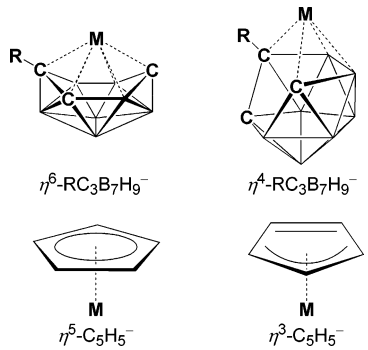

Figure 1. Comparison of the structures and bonding modes of the tricarbadecaboranyl and cyclopentadienyl monoanions.

(1) (a) Plumb, C. A.; Carroll, P. J.; Sneddon, L. G. *Organometallics* **1992**, *11*, 1665−1671. (b) Plumb, C. A.; Carroll, P. J.; Sneddon, L. G. *Organometallics* **1992**, *11*, 1672−1680. (c) Barnum, B. A.; Carroll, P. J.; Sneddon, L. G. *Organometallics* **1996**, *15*, 645−654. (d) Weinmann, W.; Wolf, A.; Pritzkow, H.; Siebert, W.; Barnum, B. A.; Carroll, P. J.; Sneddon, L. G. *Organometallics* **1995**, *14*, 1911−1919. (e) Barnum, B. A.; Carroll, P. J.; Sneddon, L. G. *Inorg. Chem.* **1997**, *36*, 1327−1337. (f) Müller, T.; Kadlecek, D. E.; Carroll, P. J.; Sneddon, L. G.; Siebert, W. *J. Organomet. Chem.* **2000**, *614*−*615*, 125−130. (g) Wasczcak, M. D.; Wang, Y.; Garg, A.; Geiger, W. E.; Kang, S. O.; Carroll, P. J.; Sneddon, L. G. *J. Am. Chem. Soc.* **2001**, *123*, 2783−2790. (h) Ramachandran, B. M.; Carroll, P. J.; Sneddon, L. G. *Inorg. Chem.* **2004**, *43*, 3467−3474. (i) Ramachandran, B. M.; Carroll, P. J.; Sneddon, L. G. *J. Am. Chem. Soc.* **2000**, *122*, 11033−11034. (j) Ramachandran, B. M.; Trupia, S. M.; Geiger, W. E.; Carroll, P. J.; Sneddon, L. G. *Organometallics* **2002**, *21*, 5078−5090.

(2) Kang, S. O.; Furst, G. T.; Sneddon, L. G *Inorg. Chem.* **1989**, *28*, 2339−2347.

10.1021/ja062201u CCC: $33.50

Table 1. NMR Data

compd	nucleus	δ (multiplicity, J (Hz), assignment)
2	$^{11}B^{a,c}$	11.4 (d, 162, 1B), 5.5 (d, 142, 1B), 4.6 (d, 147, 1B), 0.3 (d, 149, 1B), −14.4 (d, 150, 1B), −18.2 (d, 159, 1B), −27.2 (d, 162, 1B)
	$^{1}H^{a,d}$	7.03−7.45 (Ph), 6.52 (s, C3H), 2.35 (s, C4H)
3	$^{11}B^{a,c}$	4.7 (d, 157, 1B), 1.8 (d, 173, 1B), −0.4 (d, 149, 1B), −4.1 (d, 151, 1B), −18.7 (d, 149, 1B), −20.5 (d, 162, 1B), −31.1 (d, 159, 1B)
	$^{1}H^{a,d}$	6.90−7.23 (Ph), 6.29 (s, C3H), 2.60 (s, C4H)
4	$^{11}B^{a,c}$	6.8 (d, 137, 1B), 4.8 (d, 129, 1B), −1.4 (d, 133, 1B), −9.7 (d, 139, 1B), −13.7 (d, 175, 1B), −20.5 (d, 140, 1B), −21.2 (d, 165, 1B)
	$^{1}H^{a,d}$	6.93−7.27 (Ph), 3.33 (s, CH), 2.35 (s, CH), 0.89 (s, Bu^t)
5	$^{11}B^{a,c}$	6.4 (d, 136, 1B), 2.1 (d, 129, 1B), −3.3 (d, 134, 1B), −11.9 (d, 138, 1B), −15.6 (d, 146, 1B), −23.2 (d, 150, 1B), −24.1 (d, 150, 1B)
	$^{1}H^{a,d}$	6.96−7.23 (Ph), 3.35 (s, CH), 2.74 (s, CH), 0.94 (s, Bu^t)
6	$^{11}B^{e,f}$	4.0 (d, 160, 1B), 1.4 (d, 171, 1B), −2.5 (d, 141, 1B), −8.0 (d, 153, 1B), −24.5 (d, 145, 1B), −25.8 (d, 160, 1B), −33.8 (d, 160, 1B)
	$^{1}H^{e,g}$	7.23−7.60 (Ph), 6.23 (s, C3H), 2.68 (s, C4H), 1.25 (s, Bu^t)
7	$^{11}B^{a,c}$	4.6 (d, 144, 1B), 1.3 (d, 150, 1B), −0.2 (d, 150, 1B), −3.0 (d, 145, 1B), −20.6 (d, 140, 1B), −24.7 (d, 146, 1B), −32.9 (d, 153, 1B)
	$^{1}H^{a,d}$	7.05−7.72 (Ph), 5.38 (d, 24, C3H), 2.06 (s, C4H), 0.93 (d, 10, Me)
8	$^{11}B^{b,c}$	5.2 (d, 145, 1B), 1.8 (d, 125, 2B), 0.4 (d, 120, 1B), −18.6 (d, 145, 1B), −22.5 (d, 139, 1B), −30.8 (d, 148, 1B)
	$^{1}H^{b,d}$	7.28−7.80 (Ph), 5.59 (d, 23, C3H), 2.34 (s, C4H)
9	$^{11}B^{a,c}$	4.9 (d, 155, 1B), 1.7 (d, 154, 1B), −4.1 (d, 141, 1B), −7.4 (d, 149, 1B), −25.3 (d, 145, 1B), −26.3 (d, 165, 1B), −31.4 (d, 154, 1B)
	$^{1}H^{a,d}$	6.96−7.40 (Ph), 5.06 (d, 15, C3H), 2.06 (s, C4H), 0.95 (d, 10, Me)
10	$^{11}B^{b,c}$	4.4 (d,[h]1B), 2.4 (d, 149, 1B). −1.1 (d, 133, 1B), −3.4 (d, 128, 1B), −22.0 (d, 135, 2B), −30.5 (d, 137, 1B)−30.5 (d, 137, 1B)
	$^{1}H^{b,d}$	7.20−7.61 (Ph), 5.57 (d, 17, C3H), 2.69 (s, C4H)
11	$^{11}B^{e,f}$	−0.4 (d, 140, 1B), −6.9 (d, 139, 1B), −9.0 (d, 141, 1B), −13.7 (d, 130, 1B), −15.4 (d, 170, 1B), −22.1 (d, 145, 1B), −31.4 (d, 139, 1B)
	$^{1}H^{e,g}$	6.95−7.12 (Ph), 2.92 (s, CH), 1.95 (d, 9, Me), 1.92 (d, 9, Me), 1.54 (d, 13, CH)
12	$^{11}B^{e,f}$	7.5 (d, 144, 1B), −1.5 (d, 148, 1B), −8.8 (d, 132, 1B), −18.8 (d, 142, 1B), −26.0 (d, 146, 1B), −31.6 (d, 130, 1B), −32.6 (d, 170, 1B)
	$^{1}H^{e,g}$	6.97−7.82 (Ph), 3.69 (s, C3H), 1.65 (d, 9, Me), 1.54 (d, 10, Me), 1.50 (d, 22, C4H)

[a] In C_6D_6. [b] In CD_2Cl_2. [c] 160.5 MHz. [d] 500.1 MHz. [e] In $CDCl_3$. [f] 128.4 MHz. [g] 400.1 MHz. [h] Broad; coupling constant could not be determined.

some metallacyclopentadienyl[3] and metalladicarbaborane[4] complexes (Figure 1).[5] We also suggested[1i,j] that, since the $\eta^6-\eta^4$ process was more facile than the $\eta^5-\eta^3$ process, metallatricarbadecaboranyl complexes may exhibit enhanced reactivities compared to their cyclopentadienyl counterparts. In this paper, we report synthetic, structural, and chemical studies of manganese and rhenium tricarbadecaboranyl tricarbonyl complexes and demonstrate that these complexes undergo facile carbonyl substitution reactions with isocyanide and phosphines by an associative process involving cage-slipped η^4-coordinated intermediates.

Experimental Section

General Synthetic Procedures and Materials. Unless otherwise noted, all reactions and manipulations were performed in dry glassware under a nitrogen or argon atmosphere using the high-vacuum or inert-atmosphere techniques described by Shriver.[6]

The Li^+[6-Ph-*nido*-5,6,9-$C_3B_7H_9^-$] (**1**$^-$)[1h] and [(η^6-$C_{10}H_8$)$Mn(CO)_3^+$]-[BF_4^-][7] were prepared by the reported methods. $Re(CO)_5Br$ (Strem), $P(CH_3)_3$, $P(C_6H_5)_3$, *tert*-butylisocyanide (Aldrich), spectrochemical grade diethyl ether, dichloromethane, *n*-pentane, and hexanes (Fisher) were used as received. Glyme and tetrahydrofuran (Fisher) were freshly distilled from sodium benzophenone ketyl prior to use. All other solvents were used as received unless noted otherwise. The yields of all metallatricarbaborane products are calculated on the basis of the starting metal reagents.

Physical Methods. ^{11}B NMR spectra at 128.4 MHz and ^{1}H NMR spectra at 400.1 MHz were obtained on a Bruker DMX-400 spectrometer equipped with appropriate decoupling accessories. ^{11}B NMR spectra at 160.5 MHz, ^{13}C NMR spectra at 125.7 MHz, and ^{1}H NMR spectra at 500.1 MHz were obtained on a Bruker AM-500 spectrometer equipped with the appropriate decoupling accessories. All ^{11}B chemical shifts are referenced to $BF_3{\cdot}OEt_2$ (0.0 ppm), with a negative sign indicating an upfield shift. All proton chemical shifts were measured relative to internal residual protons from the lock solvents (99.5% C_6D_6 and 99.9% CD_2Cl_2) and then referenced to $(CH_3)_4Si$ (0.0 ppm). NMR data are summarized in Table 1. Photolyses were performed in Pyrex vessels using a 450 W medium-pressure Hanovia lamp at 25 °C. High- and low-resolution mass spectra, employing chemical ionization with negative ion detection, were obtained on a Micromass AutoSpec high-resolution mass spectrometer. IR spectra were obtained on a Perkin-Elmer System 2000 FTIR spectrometer. Elemental analyses were carried out at Robertson Microlit Laboratories in Madison, NJ. Melting points were determined using a standard melting point apparatus and are uncorrected.

Synthesis of 1,1,1-$(CO)_3$-2-Ph-*closo*-1,2,3,4-$MnC_3B_7H_9$ (2). A glyme solution of Li^+[6-Ph-*nido*-5,6,9-$C_3B_7H_9^-$] (**1**$^-$) (3.0 mL of a 0.5 M solution, 1.5 mmol) was added dropwise to a stirring glyme (35 mL) solution of $Mn(CO)_5Br$ (412 mg, 1.5 mmol). After being stirred for 12 h at room temperature, the deep red solution was exposed to air and filtered through a short plug of silica gel. The silica gel was washed with diethyl ether to extract any remaining product. The solvent was vacuum evaporated from the filtrate to give a dark red residue, which was then redissolved in *n*-pentane and eluted through a silica gel column with 100% *n*-pentane as the eluent. The first red band was collected, and the solvent was vacuum evaporated to yield a red powder. The product was further purified by recrystallization from *n*-pentane at −78 °C to give the red-orange product. For **2**: 1,1,1-$(CO)_3$-2-Ph-*closo*-1,2,3,4-$MnC_3B_7H_9$, yield 26% (130 mg, 0.39 mmol); red-orange; mp 66 °C. Anal. Calcd: C, 42.79; H, 4.19. Found: C, 42.37; H, 4.41. LRMS: *m*/*z* calcd for $^{12}C_{11}{}^{1}H_{14}{}^{11}B_7{}^{16}O_2{}^{55}Mn^-$ (P−CO) 310, found 310.

(3) For some examples, see: (a) Basolo, F. *New J. Chem.* **1994**, *18*, 19−24 and references therein. (b) Basolo, F. *Polyhedron* **1990**, *9*, 1503−1535 and references therein. (c) O'Connor, J. M.; Casey, C. P. *Chem. Rev.* **1987**, *87*, 307−318 and references therein. (d) Schuster-Woldan, H. G.; Basolo, F. *J. Am. Chem. Soc.* **1966**, *88*, 1657−1663. (e) Rerek, M. E.; Basolo, F. *J. Am. Chem. Soc.* **1984**, *106*, 5908−5912. (f) Simanko, W.; Tesch, W.; Sapunov, V. N.; Mereiter, K.; Schmid, R.; Kirchner, K.; Coddington, J.; Wherland, S. *Organometallics* **1998**, *17*, 5674−5688. (g) Calhorda, M. J.; Gamelas, C. A.; Romão, C. C.; Veiros, L. F. *Eur. J. Inorg. Chem.* **2000**, 331−340.

(4) Shen, J. K.; Zhang, S.; Basolo, F.; Johnson, S. E.; Hawthorne, M. F. *Inorg. Chim. Acta* **1995**, *235*, 89−97.

(5) For more examples of cage-slipped metalladicarbaboranes, see: (a) Hawthorne, M. F.; Dunks, G. B. *Science* **1972**, *178*, 462−471. (b) Warren, L. F.; Hawthorne, M. F. *J. Am. Chem. Soc.* **1968**, *90*, 4823−4828. (c) Warren, L. F.; Hawthorne, M. F. *J. Am. Chem. Soc.* **1970**, *92*, 1157−1173.

(6) Shriver, D. F.; Drezdzon, M. A. *The Manipulation of Air-Sensitive Compounds*, 2nd ed.; Wiley: New York, 1986.

(7) Sun, S.; Yeung, L. K.; Sweigart, D. A.; Lee, T.-Y.; Lee, S. S.; Chung, Y. K.; Switzer, S. R.; Pike, R. D. *Organometallics* **1995**, *14*, 2613−2615.

IR (KBr, cm^{-1}): 2963 (s), 2566 (s), 2051 (vs), 2002 (vs), 1964 (vs), 1801 (w), 1582 (w), 1498 (m), 1449 (s), 1261 (s), 1091 (m), 794 (m), 649 (w).

Alternate Synthesis of 1,1,1-$(CO)_3$-2-Ph-*closo*-1,2,3,4-$MnC_3B_7H_9$ (2). A glyme solution of $\mathbf{1}^-$ (4.6 mL of a 0.5 M solution, 2.3 mmol) was added dropwise to a stirring yellow suspension of [(η^6-$C_{10}H_8$)-$Mn(CO)_3^+$][BF_4^-] (797 mg, 2.3 mmol) in CH_2Cl_2 (25 mL). After being stirred for 2 h at room temperature, the deep red solution was exposed to air, and the product was worked up as described above. The red-orange material, obtained in 42% yield (322 mg, 0.96 mmol), was identified by its ^{11}B NMR and ^1H NMR spectra, mass spectrum, and melting point.

1,1,1-$(CO)_3$-2-Ph-*closo*-1,2,3,4-$ReC_3B_7H_9$ (3). $Re(CO)_5Br$ (1088 mg, 2.68 mmol) was dissolved in THF (60 mL) and heated at reflux for 16 h. The pale yellow solution was then cooled, a glyme solution of $\mathbf{1}^-$ (3.8 mL of a 0.70 M solution, 2.68 mmol) was added, and the mixture was refluxed for 4 h. The gold-colored solution was exposed to air and filtered through a plug of silica gel, and then the filtrate solvent was vacuum evaporated. The resulting oil was redissolved in CH_2Cl_2 and eluted through a silica gel column with 10:1 *n*-pentane:CH_2Cl_2 as the eluent. The first gold band was collected, and the solvent was vacuum evaporated to yield a gold powder. The product was further purified by recrystallization from *n*-pentane at −78 °C. For **3**: 1,1,1-$(CO)_3$-2-Ph-*closo*-1,2,3,4-$ReC_3B_7H_9$, yield 40.7% (510 mg, 1.09 mmol); gold; mp 99.5 °C. Anal. Calcd: C, 30.79; H, 3.01. Found: C, 31.01; H, 2.83. HRMS: *m*/*z* calcd for $^{12}C_{12}{}^1H_{14}{}^{11}B_7{}^{16}O_3{}^{187}Re^-$ 470.1154, found 470.1167. IR (KBr, cm^{-1}): 3064 (w), 2612 (m), 2595 (m), 2568 (m), 2063 (vs), 2055 (vs), 1997 (vs), 1947 (vs), 1119 (w), 935 (w), 692 (w), 607 (w).

8-($CNBu^t$)-8,8,8-$(CO)_3$-9-Ph-*nido*-8,7,9,10-$MnC_3B_7H_9$ (4). $CNBu^t$ (0.04 mL, 0.33 mmol) was added dropwise to a stirring *n*-pentane (2 mL) solution of **2** (100 mg, 0.30 mmol) at room temperature in air, resulting in an immediate color change from deep red to yellow and the formation of a yellow precipitate. The solution was cooled at −78 °C to completely precipitate the product, which was then filtered to yield a yellow powder. For **4**: 8-($CNBu^t$)-8,8,8-$(CO)_3$-9-Ph-*nido*-8,7,9,-10-$MnC_3B_7H_9$, yield 94.2% (118 mg, 0.28 mmol); yellow; mp 87.0 °C (dec). Anal. Calcd: C, 48.62; H, 5.52; N, 3.34. Found: C, 48.71; H, 5.64; N, 3.33. LRMS: *m*/*z* calcd for $^{12}C_{11}{}^1H_{14}{}^{11}B_7{}^{55}Mn^{16}O_2^-$ (P−$CNBu^t$, −CO) 310, found 310. IR (KBr, cm^{-1}): 2987 (m), 2594 (m), 2550 (s), 2187 (s), 2055 (vs), 2000 (vs), 1992 (vs), 1194 (m).

Re-formation of 2 from 4. A CH_2Cl_2 solution of **4** was vacuum evaporated, and the resulting yellow powder was dried in vacuo overnight. The ^{11}B NMR spectrum of a CH_2Cl_2 solution of the resulting red powder was identical to that of **2**.

Attempted Synthesis of 1-($CNBu^t$)-1,1-$(CO)_2$-2-Ph-*closo*-1,2,3,4-$MnC_3B_7H_9$. Photolytic treatment of a CH_2Cl_2 (10 mL) solution of **4** (84 mg, 0.20 mmol) at room temperature under a flow of Ar for 1 h resulted in a color change from yellow to brown. The ^{11}B NMR spectrum consisted of seven equal intensity peaks (2.4, 0.4, −0.5, −5.0, −23.8, −27.2, −33.7 ppm) and indicated the formation of an η^6-coordinated complex; however, because of fast decomposition, the product could not be isolated.

8-($CNBu^t$)-8,8,8-$(CO)_3$-9-Ph-*nido*-8,7,9,10-$ReC_3B_7H_9$ (5). $CNBu^t$ (0.03 mL, 0.23 mmol) was added dropwise to a stirring *n*-pentane (2 mL) solution of **3** (100 mg, 0.21 mmol) at room temperature in air, resulting in an immediate color change from yellow-gold to yellow and the formation of a yellow precipitate. The solution was cooled at −78 °C to completely precipitate the product, which was then filtered to yield a yellow powder. For **5**: 8-($CNBu^t$)-8,8,8-$(CO)_3$-9-Ph-*nido*-8,7,9,10-$ReC_3B_7H_9$, yield 88.3% (104 mg, 0.19 mmol); yellow; mp 137.0 °C (dec). Anal. Calcd: C, 37.04; H, 4.21; N, 2.54. Found: C, 37.25; H, 3.99; N, 2.59. LRMS: *m*/*z* calcd for $^{12}C_{12}{}^1H_{14}{}^{11}B_7{}^{16}O_3{}^{187}Re^-$ (P−$CNBu^t$) 470, found 470. IR (KBr, cm^{-1}): 2989 (w), 2583 (m), 2552 (s), 2202 (s), 2059 (vs), 2000 (vs), 1979 (vs), 1192 (m).

Re-formation of 3 from 5. A CH_2Cl_2 solution of **5** was vacuum evaporated, and the resulting yellow powder was dried in vacuo overnight. The ^{11}B NMR spectrum of a CH_2Cl_2 solution of the resulting gold-colored powder was identical to that of **3**.

1-($CNBu^t$)-1,1-$(CO)_2$-2-Ph-*closo*-1,2,3,4-$ReC_3B_7H_9$ (6). Photolytic treatment of a CH_2Cl_2 (10 mL) solution of **5** (50 mg, 0.09 mmol) at room temperature under a flow of Ar for 1 h resulted in a color change from yellow to orange. The solvent was vacuum evaporated, and the resulting orange oil was chromatographed on a TLC plate (3:1 *n*-pentane/CH_2Cl_2 eluent) to give **6** (R_f = 0.66) and other unidentified minor bands. For **6**: 1-($CNBu^t$)-1,1-$(CO)_2$-2-Ph-*closo*-1,2,3,4-$ReC_3B_7H_9$, yield 75.9% (36 mg, 0.07 mmol); orange; mp 101.0 °C. Anal. Calcd: C, 36.73; H, 4.43; N, 2.68. Found: C, 36.87; H, 4.21; N, 2.70. HRMS *m*/*z* calcd for $^{12}C_{16}{}^1H_{23}{}^{11}B_7{}^{14}N^{16}O_2{}^{187}Re^-$ 525.1937, found 525.1924. IR (KBr, cm^{-1}) 2987 (w), 2566 (s), 2178 (vs), 2001 (vs), 1915 (vs), 1496 (w), 1447 (w), 1372 (w), 1204 (m), 1115 (w), 939 (w), 747 (w), 695 (m).

1,1-$(CO)_2$-1-$P(CH_3)_3$-2-Ph-*closo*-1,2,3,4-$MnC_3B_7H_9$ (7). A THF solution of $P(CH_3)_3$ (0.60 mL of a 1.0 M solution, 0.60 mmol) was added dropwise to a stirring *n*-pentane (10 mL) solution of **2** (100 mg, 0.30 mmol) at room temperature in air, resulting in an immediate color change from red to red-brown. The solution was filtered through Celite, and slow evaporation of the filtrate solvent gave dark red-brown colored crystals. For **7**: 1,1-$(CO)_2$-1-$P(CH_3)_3$-2-Ph-*closo*-1,2,3,4-$MnC_3B_7H_9$, yield 84.3% (96 mg, 0.25 mmol); dark red-brown; mp 139.5 °C. Anal. Calcd: C, 43.68; H, 6.02. Found: C, 43.61; H, 5.87. HRMS: *m*/*z* calcd for $^{12}C_{11}{}^1H_{14}{}^{11}B_7{}^{55}Mn^{16}O_2^-$ (P−$P(CH_3)_3$) 310.1026, found 310.1076. IR (KBr, cm^{-1}): 2919 (w), 2614 (m), 2583 (m), 2548 (s), 1991 (vs), 1916 (vs), 1294 (w), 1124 (w), 949 (s), 860 (w), 737 (w), 696 (w), 672 (w).

1,1-$(CO)_2$-1-$P(C_6H_5)_3$-2-Ph-*closo*-1,2,3,4-$MnC_3B_7H_9$ (8). A CH_2Cl_2 (2 mL) solution of $P(C_6H_5)_3$ (77 mg, 0.30 mmol) and **2** (100 mg, 0.30 mmol) was stirred for 12 h at room temperature in air, resulting in a color change from dark red to brown. Addition of *n*-pentane precipitated a brown powder, which was then filtered and washed with additional *n*-pentane. For **8**: 1,1-$(CO)_2$-1-$P(C_6H_5)_3$-2-Ph-*closo*-1,2,3,4-$MnC_3B_7H_9$, yield 73.1% (124 mg, 0.22 mmol); brown; mp 146.0 °C. Anal. Calcd: C, 60.99; H, 5.12. Found: C, 60.90; H, 4.92. HRMS: *m*/*z* calcd for $^{12}C_{11}{}^1H_{14}{}^{11}B_7{}^{55}Mn^{16}O_2^-$ (P−$P(C_6H_5)_3$) 310.1026, found 310.1023. IR (KBr, cm^{-1}): 3058 (w), 2567 (s), 1991 (vs), 1918 (vs), 1435 (m), 1092 (w), 744 (w), 693 (m).

1,1-$(CO)_2$-1-$P(CH_3)_3$-2-Ph-*closo*-1,2,3,4-$ReC_3B_7H_9$ (9). A THF solution of $P(CH_3)_3$ (0.21 mL of a 1.0 M solution, 0.21 mmol) was added dropwise to a stirring CH_2Cl_2 (2 mL) solution of **3** (100 mg, 0.21 mmol) at room temperature in air, resulting in an immediate color change from gold to bright yellow, which then faded to orange after 5 min. Addition of *n*-pentane precipitated an orange powder that was then filtered and washed with additional *n*-pentane. For **9**: 1,1-$(CO)_2$-1-$P(CH_3)_3$-2-Ph-*closo*-$ReC_3B_7H_9$, yield 93.9% (104 mg, 0.20 mmol); orange; mp 188.0 °C. Anal. Calcd: C, 32.58; H, 4.49. Found: C, 31.95; H, 4.20. HRMS: *m*/*z* calcd for $^{12}C_{14}{}^1H_{23}{}^{11}B_7{}^{16}O_2{}^{31}P^{187}Re^-$ 518.1644, found 518.1622. IR (KBr, cm^{-1}): 2570 (s), 1994 (vs), 1876 (vs), 1293 (w), 942 (m).

1,1-$(CO)_2$-1-$P(C_6H_5)_3$-2-Ph-*closo*-1,2,3,4-$ReC_3B_7H_9$ (10). A CH_2Cl_2 (2 mL) solution of $P(C_6H_5)_3$ (56 mg, 0.21 mmol) and **3** (100 mg, 0.21 mmol) was stirred for 12 h at room temperature in air, resulting in a color change from gold to orange. Addition of *n*-pentane precipitated an orange powder, which was then filtered and washed with additional *n*-pentane. For **10**: 1,1-$(CO)_2$-1-$P(C_6H_5)_3$-2-Ph-*closo*-1,2,3,4-$ReC_3B_7H_9$, yield 93.1% (140 mg, 0.20 mmol); orange; mp 253.0 °C. Anal. Calcd: C, 49.59; H, 4.16. Found: C, 49.23; H, 3.91. LRMS: *m*/*z* calcd for $^{12}C_{11}{}^1H_{14}{}^{11}B_7{}^{16}O_2{}^{31}P^{187}Re^-$ (P−$P(C_6H_5)_3$) 442, found 442. IR (KBr, cm^{-1}): 3059 (w), 2565 (m), 1996 (vs), 1903 (vs), 1435 (m), 1094 (w), 744 (w), 693 (m).

8,8-$(CO)_2$-8,8-$(P(CH_3)_3)_2$-9-Ph-*nido*-8,7,9,10-$ReC_3B_7H_9$ (11). A THF solution of $P(CH_3)_3$ (0.21 mL of a 1.0 M solution, 0.21 mmol)

was added dropwise to a stirring CH_2Cl_2 (2 mL) solution of **9** (100 mg, 0.21 mmol) at room temperature in air, resulting in an immediate color change from orange to dull yellow. Addition of *n*-pentane precipitated a yellow powder that was then filtered and washed with additional *n*-pentane. For **11**: 8,8-$(CO)_2$-8,8-$(P(CH_3)_3)_2$-9-Ph-*nido*-8,7,9,10-$ReC_3B_7H_9$, yield 87.4% (100 mg, 0.17 mmol); yellow; mp 140.0 °C (dec). Anal. Calcd: C, 34.48; H, 5.45. Found: C, 34.39; H, 5.18. HRMS: *m*/*z* calcd for $^{12}C_{14}{}^{1}H_{23}{}^{11}B_7{}^{16}O_2{}^{31}P^{187}Re^-$ (P−P$(CH_3)_3$) 518.1644, found 518.1630. IR (KBr, cm^{-1}): 2916 (w), 2548 (s), 1981 (vs), 1903 (vs), 1426 (w), 1292 (w), 952 (s).

1-CO-1,1-$(P(CH_3)_3)_2$-2-Ph-*closo*-1,2,3,4-$ReC_3B_7H_9$ (12). Photolytic treatment of a CH_2Cl_2 (2 mL) solution of **11** (100 mg, 0.17 mmol) at room temperature under a flow of Ar for 5 h resulted in a color change from yellow to orange. The solvent was then vacuum evaporated, resulting in a dark orange oil. The oil was then chromatographed on a TLC plate (toluene eluent) to give **12** ($R_f = 0.55$), **11** ($R_f = 0.65$), and **9** ($R_f = 0.76$). Compounds **11** and **9** were identified by their ^{11}B NMR shifts and melting points. For **12**: 1-CO-1,1-$(P(CH_3)_3)_2$-2-Ph-*closo*-1,2,3,4-$ReC_3B_7H_9$, yield 15.1% (14.5 mg, 0.03 mmol); dark orange; mp 192.0 °C. Anal. Calcd: C, 34.06; H, 5.72. Found: C, 33.97; H, 5.47. HRMS: *m*/*z* calcd for $^{12}C_{16}{}^{1}H_{32}{}^{11}B_7{}^{16}O^{31}P_2{}^{187}Re^-$ 566.2137, found 566.2121. IR (KBr, cm^{-1}) 2974 (w), 2911 (w), 2543 (s), 1868 (vs), 1623 (w, br), 1598 (w), 1493 (w), 1429 (m), 1420 (m), 1308 (w), 1287 (s), 1115 (w), 958 (s), 945 (s), 865 (m), 729 (m), 694 (w), 675 (m).

Crystallographic Data. Single crystals of compounds **2**−**12** were grown via slow solvent evaporation from dichloromethane or *n*-pentane solution in air.

Collection and Reduction of the Data. Crystallographic data and structure refinement information are summarized in Table 2. X-ray intensity data for **2** (Penn3186), **3** (Penn3232), **4** (Penn3233), **5** (Penn3236), **6** (Penn3259), **7** (Penn3214), **8** (Penn3235), **9** (Penn3242), **10** (Penn3239), **11** (Penn3258), and **12** (Penn3262) were collected on either Rigaku R-AXIS IIC (for **2**) or Mercury CCD area detectors employing graphite-monochromated Mo Kα radiation ($\lambda = 0.71069$ Å). Indexing was performed from a series of twelve 0.5° rotation images with exposures of 30 s and a 36 mm crystal-to-detector distance, except for **2**, where a series of 1° oscillation images with exposures of 100 s/frame and an 82 mm crystal-to-detector distance were employed. Oscillation images were processed using bioteX[8] (for **2**) and CrystalClear,[9] producing a list of unaveraged F^2 and $\sigma(F^2)$ values which were then passed to the teXsan[10] (for **2**) or CrystalStructure[11] program packages for further processing and structure solution on a Silicon Graphics Indigo R4000 computer (for **2**) or a Dell Pentium III computer. The intensity data were corrected for Lorentz and polarization effects and for absorption except for **2**, which was corrected for Lorentz and polarization effects, but not for absorption.

Solution and Refinement of the Structures. The structures were solved by direct methods (SIR92[12] (for **2**) or SIR97[13]). Refinement was by full-matrix least-squares based on F^2 using SHELXL-93[14] (for **2**) or SHELXL-97.[15] All reflections were used during refinement (values of F^2 that were experimentally negative were replaced with $F^2 = 0$).

(8) *bioteX*: A suite of Programs for the Collection, Reduction and Interpretation of Imaging Plate Data; Molecular Structure Corporation, 1995.
(9) *CrystalClear*; Rigaku Corporation, 1999.
(10) *teXsan*: Crystal Structure Analysis Package; Molecular Structure Corporation, 1985, 1992.
(11) *CrystalStructure*: Crystal Structure Analysis Package; Rigaku Corp. Rigaku/MSC, 2002.
(12) Altomare, A.; Burla, M. C.; Camalli, M.; Cascarano, M.; Giacovazzo, C.; Guagliardi, A.; Polidoro, G. *J. Appl. Crystallogr.* **1994**, *27*, 435.
(13) Altomare, A.; Burla, M. C.; Camalli, M.; Cascarano, M.; Giacovazzo, C.; Guagliardi, A.; Moliterni, A.; Polidori, G. J.; Spagna, R. *J. Appl. Crystallogr.* **1999**, *32*, 115−119.
(14) Sheldrick, G. M. *SHELXL-93*: Program for the Refinement of Crystal Structures; University of Göttingen: Germany, 1993.
(15) Sheldrick, G. M. *SHELXL-97*: Program for the Refinement of Crystal Structures; University of Göttingen: Germany, 1997.

Results and Discussion

Syntheses and Structural Characterizations of 1,1,1-$(CO)_3$-2-Ph-*closo*-1,2,3,4-$MC_3B_7H_9$ [M = Mn, Re]. Analogous to the reaction of $Tl^+[C_5H_5^-]$ with $Mn(CO)_5Cl$,[16] the room-temperature reaction of $\mathbf{1}^-$ with $Mn(CO)_5Br$ resulted in the displacement of two carbonyl groups and the bromide to give the η^6-tricarbadecaboranyl manganese tricarbonyl product, **2** (eq 1), in a 26% yield after 12 h.

$$Mn(CO)_5Br + Li^+[6\text{-Ph-}nido\text{-}5,6,9\text{-}C_3B_7H_9^-]\ (\mathbf{1}^-) \rightarrow 1,1,1\text{-}(CO)_3\text{-2-Ph-}closo\text{-}1,2,3,4\text{-}MnC_3B_7H_9\ (\mathbf{2}) + 2CO + LiBr \quad (1)$$

Alternatively, the room-temperature reaction of the naphthalene manganese tricarbonyl transfer agent,[17] $[(\eta^6\text{-}C_{10}H_8)Mn(CO)_3^+][BF_4^-]$, with $\mathbf{1}^-$ gave **2** in 42% yield in only 2 h (eq 2).

$$[(\eta^6\text{-}C_{10}H_8)Mn(CO)_3^+][BF_4^-] + Li^+[6\text{-Ph-}nido\text{-}5,6,9\text{-}C_3B_7H_9^-]\ (\mathbf{1}^-) \rightarrow 1,1,1\text{-}(CO)_3\text{-2-Ph-}closo\text{-}1,2,3,4\text{-}MnC_3B_7H_9\ (\mathbf{2}) + C_{10}H_8 + LiBF_4 \quad (2)$$

The synthesis of **3**, in 41% yield, was achieved by the reaction of $Re(CO)_3(THF)_2Br$,[18] obtained by THF reflux of $Re(CO)_5Br$ for 16 h, with $\mathbf{1}^-$ (eq 3).

$$Re(CO)_3(THF)_2Br + Li^+[6\text{-Ph-}nido\text{-}5,6,9\text{-}C_3B_7H_9^-](\mathbf{1}^-) \rightarrow 1,1,1\text{-}(CO)_3\text{-2-Ph-}closo\text{-}1,2,3,4\text{-}ReC_3B_7H_9\ (\mathbf{3}) + 2THF + LiBr \quad (3)$$

2 and **3** were easily separated in pure form from other unidentified minor products and $Mn_2(CO)_{10}$ and $Re_2(CO)_{10}$, respectively, by column chromatography. **2** and **3** are soluble in a wide variety of both polar and nonpolar organic solvents, including diethyl ether, methylene chloride, and toluene, but unlike **2**, **3** is only slightly soluble in *n*-pentane. Both **2** and **3** are air- and moisture-stable.

The ^{11}B NMR spectra (Table 1) of **2** and **3**, like those of the previously known 1,1,1-$(CO)_3$-2-Me-*closo*-1,2,3,4-$MnC_3B_7H_9$,[1a] indicate C_1 cage symmetry, showing seven doublets at chemical shifts consistent with those observed for other *closo*-1,2,3,4-$MC_3B_7H_9$ cluster systems.[1] Their ^{1}H NMR spectra each show two C−H resonances, one occurring at a higher-field shift (2.4−2.6 ppm), characteristic of a proton attached to the C4 cage atom, and the other at a lower-field shift (6.3−6.5 ppm), characteristic of a proton attached to a low-coordinate carbon adjacent to the metal (C3H).[1]

In agreement with the spectroscopic data and the predicted *closo*-electron count of their $MC_3B_7H_9$ fragments (24 skeletal electrons), crystallographic determinations of **2** and **3** confirm that the metallatricarbadecaboranyl cages adopt octadecahedral geometries (Figures 2 and 3) with the metal η^6-coordinated to, and approximately centered over, the puckered six-membered face of the tricarbadecaboranyl cage. The closest metal−cage interactions are with the two carbons that are puckered out of

(16) Nesmeyanov, A. N.; Anisimov, K. N.; Kolobova, N. E. *Izv. Akad. Nauk SSSR, Ser. Khim.* **1964**, *12*, 2220.
(17) Oh, M.; Reingold, J. A.; Carpenter, G. B.; Sweigart, D. A. *Coord. Chem. Rev.* **2004**, *248*, 561−596.
(18) Ellis, D. D.; Jelliss, P. A.; Stone, F. G. A. *Organometallics* **1999**, *18*, 4982−4994.

Table 2. Crystallographic Data Collection and Structure Refinement Information

	2	**3**	**4**	**5**	**6**	**7**	**8**	**9**	**10**	**11**	**12**
empirical formula	$C_{12}H_{14}B_7MnO_3$	$C_{12}H_{14}B_7O_3Re$	$C_{17}H_{23}B_7MnNO_3$	$C_{17}H_{23}B_7NO_3Re$	$C_{16}H_{23}B_7NO_2Re$	$C_{14}H_{23}B_7O_2PMn$	$C_{29}H_{29}B_7O_2PMn$	$C_{14}H_{23}B_7O_2PRe$	$C_{29}H_{29}B_7O_2PRe$	$C_{17}H_{32}B_7O_2P_2Re$	$C_{16}H_{32}B_7OP_2Re$
formula weight	336.84	468.10	419.97	551.23	523.22	384.90	571.10	516.16	702.36	592.24	564.23
crystal class	monoclinic	monoclinic	triclinic	triclinic	monoclinic	monoclinic	monoclinic	triclinic	monoclinic	monoclinic	orthorhombic
space group	$P2_1/n$ (No. 14)	$P2_1/n$ (No. 14)	$P\bar{1}$ (No. 2)	$P\bar{1}$ (No. 2)	$P2_1/c$ (No. 14)	$P2_1/c$ (No. 14)	$P2_1/c$ (No. 14)	$P\bar{1}$ (No. 2)	$P2_1/c$ (No. 14)	$P2_1/n$ (No. 14)	$Pbca$ (No. 61)
Z	4	4	2	2	8	4	4	2	4	4	8
a, Å	6.3968(2)	6.3488(4)	8.8158(4)	8.8235(8)	24.732(2)	14.7077(11)	13.6131(16)	6.749(2)	13.8587(11)	15.0215(7)	11.1322(7)
b, Å	14.9728(7)	15.1333(11)	10.9388(7)	11.0776(11)	9.4221(8)	10.1293(8)	10.8102(10)	9.771(4)	10.8412(9)	11.8681(5)	17.1778(12)
c, Å	16.0696(5)	16.1255(13)	11.7103(8)	11.7486(11)	17.6886(17)	14.4052(13)	20.420(2)	15.203(5)	20.6732(16)	13.6068(6)	24.5691(18)
α, deg			81.681(5)	81.348(7)				81.27(2)			
β, deg	90.262(3)	90.467(1)	76.353(5)	75.948(7)	92.614(2)	112.496(2)	108.1440(10)	80.65(2)	109.5620(10)	96.4600(10)	
γ, deg			74.378(4)	72.778(6)				83.46(2)			
V, Å^3	1539.1(1)	1549.3(2)	1052.9(1)	1060.2(2)	4117.7(7)	1982.8(3)	2855.6(5)	973.7(6)	2926.8(4)	2410.4(2)	4698.3(6)
D_{calc}, g/cm^3	1.454	2.007	1.325	1.727	1.688	1.289	1.328	1.761	1.594	1.632	1.595
μ, cm^{-1}	8.60	78.46	6.45	57.49	59.12	7.50	5.45	63.26	42.33	51.85	53.13
λ, Å (Mo Kα)	0.71069	0.71069	0.71069	0.71069	0.71069	0.71069	0.71069	0.71069	0.71069	0.71069	0.71069
crystal size, mm	0.30 × 0.24 × 0.20	0.40 × 0.12 × 0.08	0.45 × 0.15 × 0.10	0.28 × 0.12 × 0.05	0.32 × 0.28 × 0.08	0.35 × 0.20 × 0.07	0.35 × 0.24 × 0.12	0.38 × 0.10 × 0.03	0.40 × 0.10 × 0.05	0.18 × 0.07 × 0.06	0.45 × 0.08 × 0.03
F(000)	680	880	432	532	2016	792	1176	496	1376	1160	2208
2θ angle, deg	5.06−50.66	5.06−54.96	5.06−54.94	5.04−54.96	5.14−55.02	5.02−54.94	5.72−54.92	5.48−54.96	5.62−54.96	5.14−55.10	5.48−54.94
temperature, K	200	143	143	143	143	143	143	143	143	143	143
hkl collected	$-7 \le h \le 7$ $-17 \le k \le 18$ $-19 \le l \le 18$	$-8 \le h \le 7$ $-14 \le k \le 19$ $-20 \le l \le 16$	$-11 \le h \le 9$ $-13 \le k \le 14$ $-15 \le l \le 14$	$-11 \le h \le 11$ $-14 \le k \le 11$ $-15 \le l \le 13$	$-32 \le h \le 25$ $-12 \le k \le 10$ $-22 \le l \le 22$	$-18 \le h \le 17$ $-10 \le k \le 13$ $-18 \le l \le 17$	$-16 \le h \le 17$ $-14 \le k \le 10$ $-26 \le l \le 26$	$-7 \le h \le 8$ $-12 \le k \le 12$ $-19 \le l \le 17$	$-14 \le h \le 17$ $-11 \le k \le 13$ $-26 \le l \le 26$	$-18 \le h \le 19$ $-15 \le k \le 13$ $-14 \le l \le 17$	$-14 \le h \le 11$ $-22 \le k \le 20$ $-31 \le l \le 25$
no. of reflns measured	12577	9443	13126	10859	30071	13789	21210	10994	20234	48635	22896
no. of unique reflns	2785 ($R_{int} = 0.0266$)	3431 ($R_{int} = 0.0319$)	4677 ($R_{int} = 0.0261$)	4637 ($R_{int} = 0.0236$)	9333 ($R_{int} = 0.0237$)	4471 ($R_{int} = 0.0232$)	6374 ($R_{int} = 0.0296$)	4312 ($R_{int} = 0.0217$)	6591 ($R_{int} = 0.0212$)	48635 ($R_{int1} = 0.0560$, $R_{int2} = 0.0710$)[c]	5317 ($R_{int} = 0.0344$)
no. of observed reflns ($F > 4\sigma$)	2637	3131	3928	4334	8140	3922	5313	4057	6060	37296	3156
no. of reflns used in refinement	2785	3431	4677	4637	9333	4471	6374	4312	6591	48635	5317
no. of parameters	265	209	355	355	494	318	478	266	398	297	251
R[a] indices ($F > 4\sigma$)	$R_1 = 0.0365$ $wR_2 = 0.0942$	$R_1 = 0.0315$ $wR_2 = 0.0807$	$R_1 = 0.0468$ $wR_2 = 0.1355$	$R_1 = 0.0259$ $wR_2 = 0.0613$	$R_1 = 0.0249$ $wR_2 = 0.0552$	$R_1 = 0.0360$ $wR_2 = 0.0750$	$R_1 = 0.0485$ $wR_2 = 0.1403$	$R_1 = 0.0202$ $wR_2 = 0.0433$	$R_1 = 0.0250$ $wR_2 = 0.0585$	$R_1 = 0.0549$ $wR_2 = 0.1471$	$R_1 = 0.0273$ $wR_2 = 0.0455$
R[a] indices (all data)	$R_1 = 0.0391$ $wR_2 = 0.0961$	$R_1 = 0.0341$ $wR_2 = 0.0829$	$R_1 = 0.0539$ $wR_2 = 0.1427$	$R_1 = 0.0288$ $wR_2 = 0.0634$	$R_1 = 0.0300$ $wR_2 = 0.0583$	$R_1 = 0.0437$ $wR_2 = 0.0789$	$R_1 = 0.0694$ $wR_2 = 0.1992$	$R_1 = 0.0224$ $wR_2 = 0.0444$	$R_1 = 0.0284$ $wR_2 = 0.0615$	$R_1 = 0.0774$ $wR_2 = 0.1686$	$R_1 = 0.0571$ $wR_2 = 0.0517$
GOF[b]	1.058	1.069	1.086	1.093	1.011	1.080	1.108	1.097	1.062	1.112	0.841
final difference peaks, e/Å^3	+0.245, −0.319	+3.354, −2.673	+2.164, −0.308	+2.545, −1.147	+1.972, −1.709	+0.511, −0.380	+0.948, −1.068	+1.059, −0.950	+3.046, −1.297	+2.028, −1.777	+2.298, −0.997

[a] $R_1 = \sum||F_o| - |F_c||/\sum |F_o|$; $wR_2 = \{\sum w(F_o^2 - F_c^2)^2/\sum w(F_o^2)^2\}^{1/2}$. [b] GOF $= \{\sum w(F_o^2 - F_c^2)^2/(n - p)\}^{1/2}$, where n is the number of reflections and p is the number of parameters refined. [c] Twinned crystal.

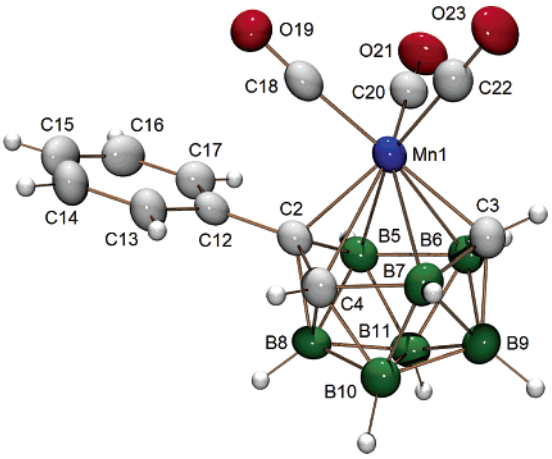

Figure 2. ORTEP representation of the structure of 1,1,1-$(CO)_3$-2-Ph-*closo*-1,2,3,4-$MnC_3B_7H_9$ (**2**). Selected distances (Å) and angles (deg): Mn1−C2, 2.096(2); Mn1−C3, 2.050(2); Mn1−C4, 2.415(2); Mn1−B5, 2.345(3); Mn1−B6, 2.342(3); Mn1−B7, 2.408(3); C2−C12, 1.490(3); C2−C4, 1.509(3); C4−B7, 1.754(4); B7−C3, 1.577(4); C3−B6, 1.561(4); B6−B5, 1.886(4); B5−C2, 1.582(3); Mn1−C18, 1.836(3); C18−O19, 1.145(3); Mn1−C20, 1.792(2); C20−O21, 1.149(3); Mn1−C22, 1.826(3); C22−O23, 1.141(3); C2−Mn1−C3, 103.7(1); Mn1−C2−C12, 123.0(2); C2−Mn1−C18, 83.1(1); C2−Mn1−C20, 108.5(1); C2−Mn1−C22, 155.9(1); C3−Mn1−C18, 153.5(1); C3−Mn1−C20, 111.1(1); C3−Mn1−C22, 80.6(1); Mn1−C18−O19, 177.1(2); Mn1−C20−O21, 177.3(2); Mn1−C22−O23, 179.4(2).

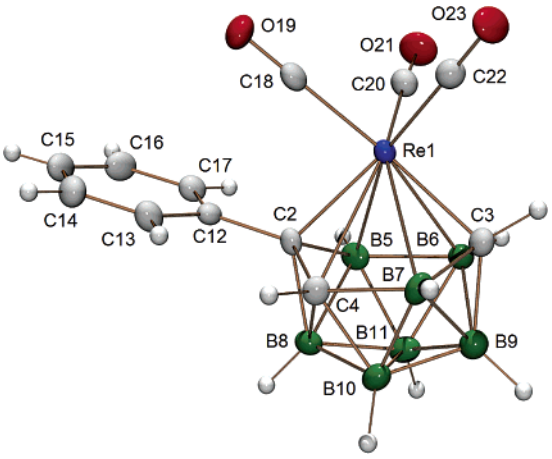

Figure 3. ORTEP representation of the structure of 1,1,1-$(CO)_3$-2-Ph-*closo*-1,2,3,4-$ReC_3B_7H_9$ (**3**). Selected distances (Å) and angles (deg): Re1−C2, 2.202(4); Re1−C3, 2.169(3); Re1−C4, 2.546(4); Re1−B5, 2.432(5); Re1−B6, 2.450(5); Re1−B7, 2.543(4); C2−C12, 1.500(5); C2−C4, 1.517(5); C4−B7, 1.772(6); B7−C3, 1.587(6); C3−B6, 1.577(7); B6−B5, 1.915(6); B5−C2, 1.602(6); Re1−C18, 1.971(4); C18−O19, 1.142(5); Re1−C20, 1.906(4); C20−O21, 1.140(5); Re1−C22, 1.953(4); C22−O23, 1.134(5); C2−Re1−C3, 98.6(2); Re1−C2−C12, 121.6(3); C2−Re1−C18, 83.7(2); C2−Re1−C20, 110.9(2); C2−Re1−C22, 155.9(1); C3−Re1−C18, 154.4(2); C3−Re1−C20, 113.3(2); C3−Re1−C22, 83.6(2); Re1−C18−O19, 178.8(4); Re1−C20−O21, 174.9(3); Re1−C22−O23, 179.5(4).

the ring, for **2** (Mn1−C2, 2.096(2) and Mn1−C3, 2.050(2) Å) and for **3** (Re1−C2, 2.202(4) and Re1−C3, 2.169(3) Å). Longer and approximately equivalent distances are observed between the metal and the remaining four atoms of the tricarbadecaboranyl bonding face, for **2** (Mn1−C4, 2.415(2); Mn1−B5, 2.345(3); Mn1−B6, 2.342(3); Mn1−B7, 2.408(3) Å) and for **3** (Re1−C4, 2.546(4); Re1−B5, 2.432(5); Re1−B6, 2.450(5); Re1−B7, 2.543(4) Å). The phenyl group in both compounds is attached to the C2 cage carbon adjacent to the metal. The M−C2 and M−C3 distances are significantly shorter than the M−C distances to the ring carbons found in the analogous (η^5-C_5H_5)-$Mn(CO)_3$[19] (2.133(3)−2.142(3) Å), (η^5-C_5Me_5)$Mn(CO)_3$[20] (2.112(7)−2.137(8) Å), (η^5-C_5H_5)$Re(CO)_3$[21] (2.280(7)−2.292(9) Å), and (η^5-C_5Me_5)$Re(CO)_3$[22] (2.286(8)−2.313(7) Å). Although there are no statistical differences between the C−O bond distances observed in **2** and **3** and those of their corresponding cyclopentadienyl counterparts, the average M−C(carbonyl) distances in **2** (1.818(3) Å) and **3** (1.943(4) Å) are longer than the M−C(carbonyl) distances in (η^5-C_5H_5)$Mn(CO)_3$ (1.793(3) Å) and (η^5-C_5Me_5)$Mn(CO)_3$ (1.725(11) Å) and in (η^5-C_5H_5)-$Re(CO)_3$ (1.894(7) Å) and (η^5-C_5Me_5)$Re(CO)_3$ (1.891(10) Å), respectively.

Consistent with the differences observed in their M−C(carbonyl) distances, the CO stretching absorptions in the IR spectrum of 1,1,1-$(CO)_3$-2-Ph-*closo*-1,2,3,4-$MnC_3B_7H_9$ are at higher energies (2051, 2002, and 1964 cm^{-1}, KBr) than those of (η^5-C_5H_5)$Mn(CO)_3$ (2027 and 1944 cm^{-1}, KBr) and (η^5-C_5Me_5)$Mn(CO)_3$ (2004 and 1910 cm^{-1}, KBr).[23] Likewise, the CO stretching absorptions in 1,1,1-$(CO)_3$-2-Ph-*closo*-1,2,3,4-$ReC_3B_7H_9$ are at higher energies (2055, 1997, and 1947 cm^{-1}, KBr) than those of (η^5-C_5H_5)$Re(CO)_3$ (2025 and 1926 cm^{-1}, KBr) and (η^5-C_5Me_5)$Re(CO)_3$ (2007 and 1909 cm^{-1}, KBr).[23] Thus, both the IR and M−C(carbonyl) bond distance data indicate that, in **2** and **3**, there is less metal-to-CO back-bonding than in their cyclopentadienyl analogues. As previously noted, this is consistent with tricarbadecaboranyl ligands being more electron-withdrawing than their cyclopentadienyl counterparts.[1a] The CO stretching absorptions of the previously synthesized 1,1,1-$(CO)_3$-2-Me-*closo*-1,2,3,4-$MnC_3B_7H_9$ (2040, 2008, and 1960 cm^{-1}, KBr) are also at lower energies than those of **2**, indicating, as noted before,[1h] that the phenyl-functionalized tricarbadecaboranyl ligand is more electron-withdrawing than the methyl derivative.

Monosubstitution Reactions. The carbonyl substitution reactions of cyclopentadienyl manganese and rhenium tricarbonyl have been extensively studied.[24] These reactions could, in principle, go by either a dissociative mechanism, involving initial dissociation of one carbonyl followed by ligand attack (eq 4), or an associative mechanism, involving coordination of the incoming ligand before loss of the carbon monoxide (eq 5).

$$(\eta^5\text{-}C_5H_5)M(CO)_3 \xrightarrow{-CO} (\eta^5\text{-}C_5H_5)M(CO)_2 \xrightarrow{L} (\eta^5\text{-}C_5H_5)M(CO)_2L \quad (4)$$

$$(\eta^5\text{-}C_5H_5)M(CO)_3 \xrightarrow{L} (\eta^3\text{-}C_5H_5)M(CO)_3L \xrightarrow{-CO} (\eta^5\text{-}C_5H_5)M(CO)_2L \quad (5)$$

The latter mechanism has been proposed to involve an η^5−η^3 ring-slippage process that both opens up a metal coordination

(19) Cowie, J.; Hamilton, E. J. M.; Laurie, J. C. V.; Welch, A. J. *J. Organomet. Chem.* **1990**, *394*, 1−13.
(20) Fortier, S.; Baird, M. C.; Preston, K. F.; Morton, J. R.; Ziegler, T.; Jaeger, T. J.; Watkins, W. C.; MacNeil, J. H.; Watson, K. A.; Hensel, K.; Le Page, Y.; Charland, J.-P.; Williams, A. J. *J. Am. Chem. Soc.* **1991**, *113*, 542−551.
(21) Fitzpatrick, P. J.; Le Page, Y.; Butler, I. S. *Acta Crystallogr.* **1981**, *B37*, 1052−1058.
(22) Huang, Y.; Butler, I. S.; Gilson, D. F. R. *Inorg. Chem.* **1992**, *31*, 4762−4765.
(23) Bencze, É.; Mink, J.; Németh, C.; Herrmann, W. A.; Lokshin, B. V.; Kühn, F. E. *J. Organomet. Chem.* **2002**, *642*, 246−258.
(24) (a) Caulton, K. G. *Coord. Chem. Rev.* **1981**, *38*, 1−43. (b) Manuel, T. A. *Adv. Organomet. Chem.* **1965**, *3*, 181−261.

site for the incoming ligand and enables the metal to maintain its 18-electron configuration following ligand association.

Because (η^5-C_5H_5)$Mn(CO)_3$ is thermally inert,[25] substitution has usually been achieved through the photolysis of the complex in a donor solvent (eq 6), followed by addition of the substituting ligand (eq 7).

$$(\eta^5\text{-}C_5H_5)Mn(CO)_3 + THF \xrightarrow{h\nu} (\eta^5\text{-}C_5H_5)Mn(CO)_2(THF) + CO \quad (6)$$

$$(\eta^5\text{-}C_5H_5)Mn(CO)_2(THF) \xrightarrow{L} (\eta^5\text{-}C_5H_5)Mn(CO)_2L \quad (7)$$

The rate of THF substitution from (η^5-C_5H_5)$Mn(CO)_2$(THF) (eq 7) was shown to be dependent upon the THF concentration but independent of the nature of the incoming ligand, L,[26] thus, indicating a dissociative process. Likewise, the thermal substitution of (η^5-$C_5H_4C(O)CH_3$)$Mn(CO)_2SC_4H_8$, (η^1:η^5-$C_5H_4C(O)CH_2SCH_3$)$Mn(CO)_2$, and (η^1:η^5-$C_5H_4C(O)CH_2CH_2SCH_3$)$Mn(CO)_2$, derivatives of (η^5-C_5H_5)$Mn(CO)_3$, by a number of phosphines and phosphites was also proposed to proceed through a dissociative pathway, because the observed rate constants were independent of both the solvent and the concentration of the incoming ligand, and the reactions were determined to have a positive entropy of activation.[27]

In contrast to the dissociative reactions described above, Basolo found that the monosubstitution reactions of (η^5-C_9H_7)-$Mn(CO)_3$ and (η^5-$C_{13}H_9$)$Mn(CO)_3$ with phosphines were second order and had large, negative entropies of activation, indicating that they were reacting via an associative mechanism involving η^3 ring-slipped intermediates.[28] Supporting such a process, Son structurally confirmed[29] that the (η^3-$C_{10}H_9$)$Mn(CO)_3P(OMe)_3$ complex was produced by the reaction of (η^5-$C_{10}H_9$)$Mn(CO)_3$ with $P(OMe)_3$ and then showed that, upon heating[29] or photolysis,[30] this complex lost CO to produce (η^5-$C_{10}H_9$)$Mn(CO)_2$P-$(OMe)_3$.

Substitution reactions of (η^5-C_5H_5)$Re(CO)_3$ have been achieved through photolytic means similar to those discussed above for (η^5-C_5H_5)$Mn(CO)_3$,[24] but (η^5-C_5H_5)$Re(CO)_3$, unlike (η^5-C_5H_5)-$Mn(CO)_3$, also readily undergoes thermally activated substitution. For example, Casey and co-workers demonstrated that the reaction of (η^5-C_5H_5)$Re(CO)_3$ with $P(CH_3)_3$ produced both *fac*-(η^1-C_5H_5)$Re(CO)_3(P(CH_3)_3)_2$ and (η^5-C_5H_5)$Re(CO)_2P(CH_3)_3$.[31] It was reported that the rate of these reactions depended on the concentration of both (η^5-C_5H_5)$Re(CO)_3$ and $P(CH_3)_3$, and therefore the formation of both (η^1-C_5H_5)$Re(CO)_3(P(CH_3)_3)_2$ and (η^5-C_5H_5)$Re(CO)_2P(CH_3)_3$ must proceed through an associative mechanism via a ring-slipped intermediate, (η^3-C_5H_5)$Re(CO)_3$P-$(CH_3)_3$.

In the reactions of 1-(η^5-C_5Me_5)-2-Me-*closo*-1,2,3,4-$RuC_3B_7H_9$ and 1-(η^5-C_5Me_5)-2-Ph-*closo*-1,2,3,4-$FeC_3B_7H_9$ with *tert*-butyl isocyanide, the addition of two electrons to the metal caused the 6-Ph-*nido*-5,6,9-$C_3B_7H_9^-$ ligand to undergo a cage-slippage process, analogous to the $\eta^5-\eta^3$ ring-slippage of the cyclopentadienyl complexes discussed above, to yield η^4-coordinated complexes (eqs 8 and 9).[1i,j]

$$1\text{-}(\eta^5\text{-}C_5Me_5)\text{-}2\text{-}Me\text{-}closo\text{-}1,2,3,4\text{-}RuC_3B_7H_9 + CNBu^t \rightarrow 8\text{-}(\eta^5\text{-}C_5Me_5)\text{-}8\text{-}(CNBu^t)\text{-}9\text{-}Me\text{-}nido\text{-}8,7,9,10\text{-}RuC_3B_7H_9 \quad (8)$$

$$1\text{-}(\eta^5\text{-}C_5Me_5)\text{-}2\text{-}Ph\text{-}closo\text{-}1,2,3,4\text{-}FeC_3B_7H_9 + CNBu^t \rightarrow 8\text{-}(\eta^5\text{-}C_5Me_5)\text{-}8\text{-}(CNBu^t)\text{-}9\text{-}Ph\text{-}nido\text{-}8,7,9,10\text{-}FeC_3B_7H_9 \quad (9)$$

It was likewise found that, when *tert*-butyl isocyanide was added to solutions of **2** and **3**, the yellow η^4 cage-slipped tricarbonyl isocyanide complexes, **4** and **5**, were produced (eq 10).

$$1,1,1\text{-}(CO)_3\text{-}2\text{-}Ph\text{-}closo\text{-}1,2,3,4\text{-}MC_3B_7H_9 + CNBu^t \rightarrow [M = Mn\ (\mathbf{2}),\ Re\ (\mathbf{3})]$$
$$8\text{-}(CNBu^t)\text{-}8,8,8\text{-}(CO)_3\text{-}9\text{-}Ph\text{-}nido\text{-}8,7,9,10\text{-}MC_3B_7H_9 [M = Mn\ (\mathbf{4}),\ Re\ (\mathbf{5})] \quad (10)$$

4 and **5** precipitated when the reaction was carried out in *n*-pentane. Both compounds are air- and moisture-stable. The ^{11}B NMR spectra (Table 1) of **4** and **5** are similar to those of 1-(η^5-C_5Me_5)-2-Me-*closo*-1,2,3,4-$RuC_3B_7H_9$ and 1-(η^5-C_5Me_5)-2-Ph-*closo*-1,2,3,4-$FeC_3B_7H_9$.[1i,j] The ^1H NMR spectra of **4** and **5** show, as in compounds **2** and **3**, a higher-field C−H resonance (2.4−2.7 ppm) and a lower-field resonance (3.3−3.4 ppm) for each hydrogen attached to a cage carbon.

The change in cage hapticity observed in these reactions, like the $\eta^5-\eta^3$ ring-slippage process, reduces the electron donation of the tricarbadecaboranyl anion from six to four electrons, thus allowing the preservation of the 18-electron count of the metal upon the association of an incoming two-electron ligand. From a skeletal electron counting viewpoint, the addition of the two-electron isocyanide ligand to **2** and **3** increases the skeletal electron count of the metallatricarbadecaboranyl fragment to 26 skeletal electrons. Therefore, **4** and **5** should adopt open-cage 11-vertex *nido* geometries, based on an icosahedron missing one vertex. Crystallographic determinations of **4** and **5** confirm the predicted *nido* (i.e., slipped cage) geometries. In principle, the metal could slip to either the C7−B3−B4−C9 face or the C9−C10−B11−C7 face of the tricarbadecaboranyl cage. However, in agreement with the known preference of carbon atoms to adopt low-coordinate positions on the open face of clusters,[32] the slip occurs such that the metals become η^4-coordinated to, and approximately centered over, the C7−B3−B4−C9 faces of the tricarbadecaboranyl cages (Figures 4 and 5), thus producing five-membered (M−C7−B11−C10−C9) open faces containing all three cage carbons. The Mn8−C7 (2.244(2) Å), Mn8−C9 (2.267(2) Å), Re8−C7 (2.308(4) Å), and Re8−C9 (2.330(4) Å) distances are longer than the analogous distances in **2** and **3**, while the Mn8−B4 (2.311(2) Å), Mn8−B3 (2.340(3) Å), Re8−B4 (2.395(4) Å), and Re8−B3 (2.420(5) Å) distances are shorter. Because of these differences and the fact that the C10 and B11 cage atoms are not within bonding distances to the metals (Mn8−C10, 3.135(2) Å; Mn8−B11, 3.146(3) Å; Re8−C10, 3.210(5) Å; Re8−

(25) Angelici, R. J.; Loewen, W. *Inorg. Chem.* **1967**, *6*, 682−686.
(26) Coleman, J. E.; Dulaney, K. E.; Bengali, A. A. *J. Organomet. Chem.* **1999**, *572*, 65−71.
(27) Pang, Z.; Johnston, R. F. *Polyhedron* **1999**, *18*, 3469−3477.
(28) Ji, L.-N.; Rerek, M. E.; Basolo, F. *Organometallics* **1984**, *3*, 740−745.
(29) Son, S. U.; Paik, S.-J.; Lee, I. S.; Lee, Y.-A.; Chung, Y. K.; Seok, W. K.; Lee, H. N. *Organometallics* **1999**, *18*, 4114−4118.
(30) Georg, A.; Kreiter, C. G. *Eur. J. Inorg. Chem.* **1999**, 651−654.
(31) Casey, C. P.; O'Connor, J. M.; Jones, W. D.; Haller, K. J. *Organometallics* **1983**, *2*, 535−538.
(32) Williams, R. E. *Adv. Inorg. Chem. Radiochem.* **1976**, *18*, 67−142.

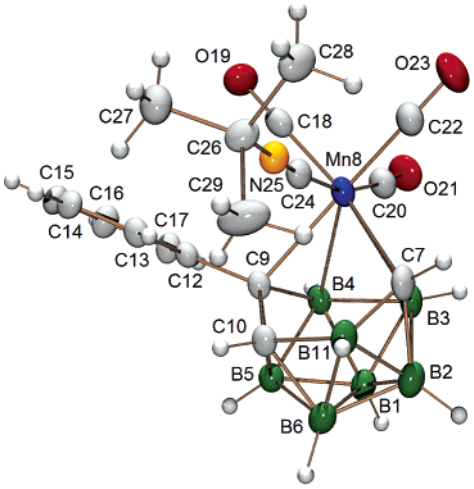

Figure 4. ORTEP representation of the structure of 8-(CNBu^t)-8,8,8-(CO)$_3$-9-Ph-*nido*-8,7,9,10-MnC$_3$B$_7$H$_9$ (**4**). Selected distances (Å) and angles (deg): Mn8−C9, 2.267(2); Mn8−C7, 2.244(2); Mn8−C10, 3.135(2); Mn8−B4, 2.311(2); Mn8−B3, 2.340(3); Mn8−B11, 3.146(3); C9−C12, 1.501(3); C9−C10; 1.518(3); C10−B11, 1.656(3); B11−C7, 1.586(3); C7−B3, 1.585(3); B3−B4, 1.924(3); B4−C9, 1.593(3); Mn8−C18, 1.838(2); C18−O19, 1.142(3); Mn8−C20, 1.840(2); C20−O21, 1.138(3); Mn8−C22, 1.832(2); C22−O23, 1.137(3); Mn8−C24, 1.974(2); C24−N25, 1.154(3); C9−Mn8−C7, 80.9(1); Mn8−C9−C12, 112.6(1); C9−Mn8−C18, 91.8-(1); C9−Mn8−C20, 110.0(1); C9−Mn8−C22, 164.1(1); C9−Mn8−C24, 81.4(1); C7−Mn8−C18, 164.0(1); C7−Mn8−C20, 110.4(1); C7−Mn8−C22, 89.6(1); C7−Mn8−C24, 78.6(1); Mn8−C18−O19, 178.9(2); Mn8−C20−O21, 175.0(2); Mn8−C22−O23, 179.2(2); Mn8−C24−N25, 175.3(2).

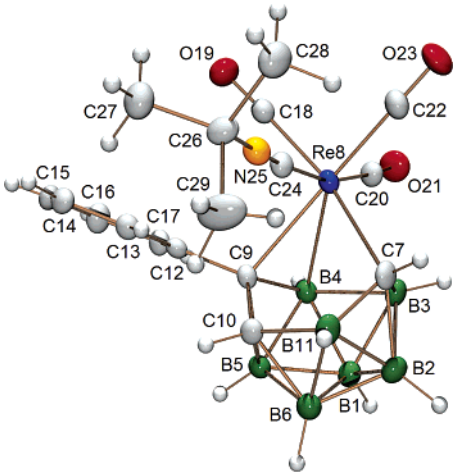

Figure 5. ORTEP representation of the structure of 8-(CNBu^t)-8,8,8-(CO)$_3$-9-Ph-*nido*-8,7,9,10-ReC$_3$B$_7$H$_9$ (**5**). Selected distances (Å) and angles (deg): Re8−C9, 2.330(4); Re8−C7, 2.308(4); Re8−C10, 3.210(5); Re8−B4, 2.395(4); Re8−B3, 2.420(5); Re8−B11, 3.229(5); C9−C12, 1.509(5); C9−C10, 1.519(5); C10−B11, 1.651(6); B11−C7, 1.593(6); C7−B3, 1.583(6); B3−B4, 1.946(6); B4−C9, 1.614(5); Re8−C18, 1.947(4); C18−O19, 1.147(5); Re8−C20, 1.967(4); C20−O21, 1.141(5); Re8−C22, 1.963-(4); C22−O23, 1.128(5); Re8−C24, 2.088(4); C24−N25, 1.160(5); C9−Re8−C7, 78.3(1); Re8−C9−C12, 112.2(2); C9−Re8−C18, 92.4(2); C9−Re8−C20, 109.6(2); C9−Re8−C22, 163.8(2); C9−Re8−C24, 81.0(1); C7−Re8−C18, 163.6(2); C7−Re8−C20, 109.4(2); C7−Re8−C22, 91.9(2); C7−Re8−C24, 78.4(2); Re8−C18−O19, 178.0(4); Re8−C20−O21, 176.4(4); Re8−C22−O23, 177.9(4); Re8−C24−N25, 175.9(3).

B11, 3.229(5) Å), the dihedral angles between the C7−M−C9 and C9−C10−B11−C7 planes in **4** (29.4(1)°) and **5** (29.3(3)°) are significantly smaller than the equivalent dihedral angle between the C2−M−C3 and C2−C4−B7−C3 planes in **2** (62.4(1)°) and **3** (61.2(1)°).

As previously observed for the ruthenium and iron systems discussed above,[1i,j] it was found that, when vacuum was applied

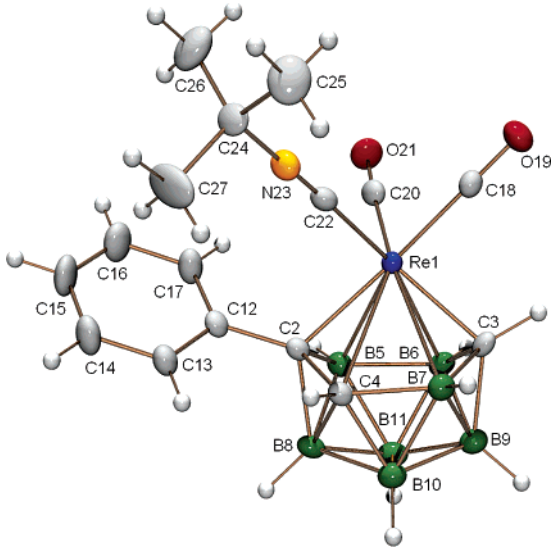

Figure 6. ORTEP representation of the structure of 1-(CNBu^t)-1,1-(CO)$_2$-2-Ph-*closo*-1,2,3,4-ReC$_3$B$_7$H$_9$ (**6**). Selected distances (Å) and angles (deg): Re1−C2, 2.200(3); Re1−C3, 2.114(3); Re1−C4, 2.559(3); Re1−B5, 2.423-(4); Re1−B6, 2.413(4); Re1−B7, 2.505(4); C2−C12, 1.506(4); C2−C4, 1.521(4); C4−B7, 1.745(5); B7−C3, 1.611(5); C3−B6, 1.605(5); B6−B5, 1.874(5); B5−C2, 1.603(5); Re1−C18, 1.945(3); C18−O19, 1.133(5); Re1−C20, 1.907(4); C20−O21, 1.151(5); Re1−C22, 2.039(3); C22−N23, 1.148-(4); C2−Re1−C3, 99.6(1); Re1−C2−C12, 122.7(2); C2−Re1−C18, 165.7(1); C2−Re1−C20, 106.6(1); C2−Re1−C22, 83.7(1); C3−Re1−C18, 83.2(1); C3−Re1−C20, 122.6(1); C3−Re1−C22, 139.9(1); Re1−C18−O19, 178.6(3); Re1−C20−O21, 176.2(3); Re1−C22−N23, 174.7(3).

to **4** and **5**, the isocyanide was lost and **2** and **3** were quantitatively re-formed (eq 11).

$$\text{8-(CNBu}^t\text{)-8,8,8-(CO)}_3\text{-9-Ph-}\textit{nido}\text{-8,7,9,10-MC}_3\text{B}_7\text{H}_9 \xrightarrow{\text{vacuum}} \text{[M = Mn (}\mathbf{4}\text{), Re (}\mathbf{5}\text{)]}$$
$$\text{1,1,1-(CO)}_3\text{-2-Ph-}\textit{closo}\text{-1,2,3,4-MC}_3\text{B}_7\text{H}_9 + \text{CNBu}^t \quad \text{[M = Mn (}\mathbf{2}\text{), Re (}\mathbf{3}\text{)]} \qquad (11)$$

On the other hand, photolysis of a CH_2Cl_2 solution of **5** for 1 h resulted in loss of CO and formation of the monosubstituted product, **6** (eq 12).

$$\text{8-(CNBu}^t\text{)-8,8,8-(CO)}_3\text{-9-Ph-}\textit{nido}\text{-8,7,9,10-ReC}_3\text{B}_7\text{H}_9 \ (\mathbf{5}) \xrightarrow{h\nu} \text{1-(CNBu}^t\text{)-1,1-(CO)}_2\text{-2-Ph-}\textit{closo}\text{-1,2,3,4-ReC}_3\text{B}_7\text{H}_9 \ (\mathbf{6}) + \text{CO} \qquad (12)$$

The ^{11}B NMR spectrum (Table 1) of **6** is similar to that of **3**. The ^{1}H spectrum of **6**, like those of **2** and **3**, shows two C−H resonances: a higher-field (2.68 ppm) peak, consistent with a proton attached to the C4 carbon, and a lower-field (6.23 ppm) peak, consistent with a proton attached to the C3 carbon.

6 is isoelectronic with **3** and should adopt a similar 11-vertex *closo* geometry. In agreement with the spectroscopic data and its predicted *closo* geometry, a crystallographic determination of **6** confirmed that the metallatricarbadecaboranyl cage adopts an octadecahedral geometry (Figure 6) with the metal again η^6-coordinated to, and approximately centered over, the puckered six-membered face of the tricarbadecaboranyl cage. The metal-to-cage distances in **6** are similar to those found in **3**, with the exception of shorter Re1−C3 (2.169(3) Å, **3**; 2.114(3)Å, **6**), Re1−B6 (2.450(5) Å, **3**; 2.413(4) Å, **6**), and Re1−B7 (2.543-

(4) Å, **3**; 2.505(4) Å, **6**) bonds. This is likely due to a trans influence of the isocyanide ligand on the cage atoms (C3, B6, and B7) trans to it through the rhenium center. There are no statistical differences between the C−O distances in **3**, **5**, and **6**, nor between the C−N distances in **5** and **6**. However, the Re1−C22 (2.039(3) Å) and average Re1−C(carbonyl) (1.926(4) Å) distances in **6** are shorter than the corresponding Re8−C24 (2.088(4) Å) and the average Re8−C(carbonyl) (1.959(5) Å) distances found in the cage-slipped compound, **5**. This is likely due to the increased steric interactions of the isocyanide ligand and three carbonyl groups in **5** compared to the isocyanide ligand and only two carbonyl groups in **6**.

In contrast to the reactions with isocyanide, the room-temperature reactions of **2** and **3** with PMe_3 and PPh_3 resulted in both phosphine addition and CO loss to form the monosubstituted dicarbonyl phosphine products, **7**−**10** (eqs 13 and 14).

$$\text{1,1,1-(CO)}_3\text{-2-Ph-}\textit{closo}\text{-1,2,3,4-MnC}_3\text{B}_7\text{H}_9\ (\mathbf{2}) + \text{PR}_3 \xrightarrow{-\text{CO}} \text{1,1-(CO)}_2\text{-1-PR}_3\text{-2-Ph-}\textit{closo}\text{-1,2,3,4-MnC}_3\text{B}_7\text{H}_9 \quad [\text{R} = \text{Me}\ (\mathbf{7}),\ \text{Ph}\ (\mathbf{8})] \quad (13)$$

$$\text{1,1,1-(CO)}_3\text{-2-Ph-}\textit{closo}\text{-1,2,3,4-ReC}_3\text{B}_7\text{H}_9\ (\mathbf{3}) + \text{PR}_3 \xrightarrow{-\text{CO}} \text{1,1-(CO)}_2\text{-1-PR}_3\text{-2-Ph-}\textit{closo}\text{-1,2,3,4-ReC}_3\text{B}_7\text{H}_9 \quad [\text{R} = \text{Me}\ (\mathbf{9}),\ \text{Ph}\ (\mathbf{10})] \quad (14)$$

Unlike for $(\eta^5\text{-C}_5\text{H}_5)\text{Mn(CO)}_3$, the carbonyl substitution reactions of **2** and **3** proceeded at room temperature in air, without the need for UV irradiation. In the case of **9**, reaction was complete in 5 min, and in the case of **7**, reaction was complete in less than 5 s!

The ^{11}B NMR spectra (Table 1) of **7**−**10** are similar to those of **2** and **3**. The ^{1}H spectra of **7**−**10**, like those of **2** and **3**, show two C−H resonances: a higher-field (2.1−2.7 ppm) peak, consistent with a proton attached to the C4 carbon, and a lower-field (5.1−5.6 ppm) peak coupled to phosphorus, consistent with a proton attached to the C3 carbon.

In agreement with both the spectroscopic data and the predicted *closo* electron count of their $MC_3B_7H_9$ fragments, crystallographic determinations of **7**−**10** confirm that the metallatricarbadecaboranyl cages still adopt octadecahedral geometries with the metals η^6-coordinated to the puckered six-membered face of the tricarbadecaboranyl cages (Figures 7−10). Other than the expected longer metal−cage distances for the rhenium compounds, the intracage distances in the tricarbadecaboranyl ligands for the manganese complexes, **7** and **8**, and the rhenium complexes, **9** and **10**, are similar. The M−B5, M−B6, M−C2, and M−C3 distances in **7**−**10** (see the captions of Figures 7−10) are much shorter than in the corresponding compounds **2** and **3** (see the captions of Figures 2 and 3), while the M−C4 and M−B7 bond distances are longer. As a result, the dihedral angles between the C2−C4−B7−C3 and the C2-M−C3 planes decrease from 62.4(1)° in **2** to 57.6(1)° in **7** and 57.2(1)° in **8** and from 61.2(1)° in **3** to 59.7(1)° in **9** and 55.8(1)° in **10**. Additionally, the metal is shifted from its position approximately centered over the six-membered open face in **2** and **3**, to a position in **7**−**10** where it is closer to the center of the C2−B5−B6−C3 plane than the C2−C4−B7−C3 plane. Probably due to steric constraints, the phosphine ligands in **7**−**10** are situated opposite the phenyl cage subsituent. There are only

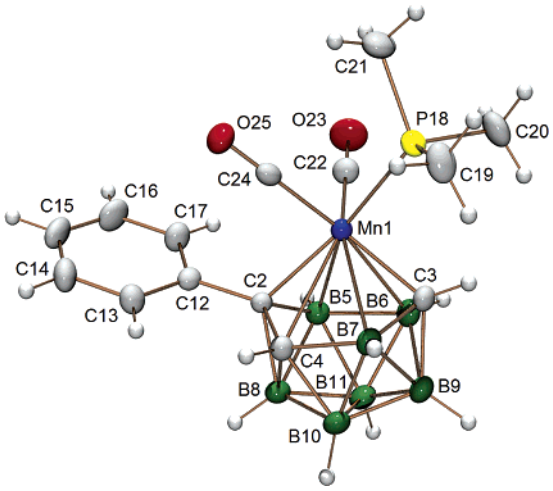

Figure 7. ORTEP representation of the structure of 1,1-$(CO)_2$-1-$P(CH_3)_3$-2-Ph-*closo*-1,2,3,4-$MnC_3B_7H_9$ (**7**). Selected distances (Å) and angles (deg): Mn1−C2, 2.079(2); Mn1−C3, 2.013(2); Mn1−C4, 2.478(2); Mn1−B5, 2.282(2); Mn1−B6, 2.297(2); Mn1−B7, 2.416(2); C2−C12, 1.495(2); C2−C4, 1.506(2); C4−B7, 1.727(3); B7−C3, 1.579(3); C3−B6, 1.580(3); B6−B5, 1.860(3); B5−C2, 1.585(3); Mn1−P18, 2.284(1); Mn1−C22, 1.769(2); C22−O23, 1.152(2); Mn1−C24, 1.826(2); C24−O25, 1.142(2); C2−Mn1−C3, 103.7(1); Mn1−C2−C12, 123.6(1); C2−Mn1−P18, 161.9(1); C2−Mn1−C22, 105.1(1); C2−Mn1−C24, 82.5(1); C3−Mn1−P18, 81.2(1); C3−Mn1−C22, 120.5(1); C3−Mn1−C24, 144.4(1); Mn1−C22−O23, 179.5(2); Mn1−C24−O25, 179.0(2).

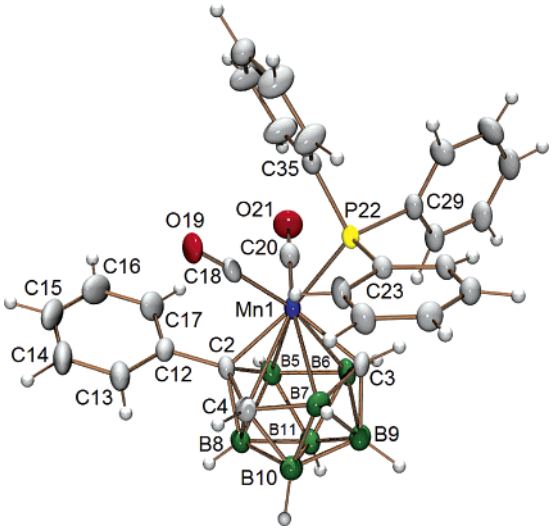

Figure 8. ORTEP representation of the structure of 1,1-$(CO)_2$-1-$P(C_5H_6)_3$-2-Ph-*closo*-1,2,3,4-$MnC_3B_7H_9$ (**8**). Selected distances (Å) and angles (deg): Mn1−C2, 2.080(2); Mn1−C3, 2.012(2); Mn1−C4, 2.499(3); Mn1−B5, 2.305(3); Mn1−B6, 2.309(3); Mn1−B7, 2.419(3); C2−C12, 1.499(3); C2−C4, 1.510(3); C4−B7, 1.726(4); B7−C3, 1.585(4); C3−B6, 1.585(4); B6−B5, 1.857(4); B5−C2, 1.589(4); Mn1−C18, 1.842(3); C18−O19, 1.131(3); Mn1−C20, 1.771(3); C20−O21, 1.157(3); Mn1−P22, 2.313(1); C2−Mn1−C3, 103.5(1); Mn1−C2−C12, 124.2(2); C2−Mn1−C18, 81.4(1); C2−Mn1−C20, 101.8(1); C2−Mn1−P22, 161.6(1); C3−Mn1−C18, 141.2(1); C3−Mn1−C20, 121.9(1); C3−Mn1−P22, 83.1(1); Mn1−C18−O19, 177.5(2); Mn1−C20−O21, 177.7(2).

small differences among complexes **7**−**10** in their metal−cage and intracage distances, even though the cone angles differ significantly for the two phosphines (118° for PMe_3 and 145° for PPh_3).[33]

No intermediate species were observed by ^{11}B NMR spectroscopy at room temperature in the reaction of **2** with PMe_3,

(33) Tolman, C. A. *Chem. Rev.* **1977**, *77*, 313−348 and references therein.

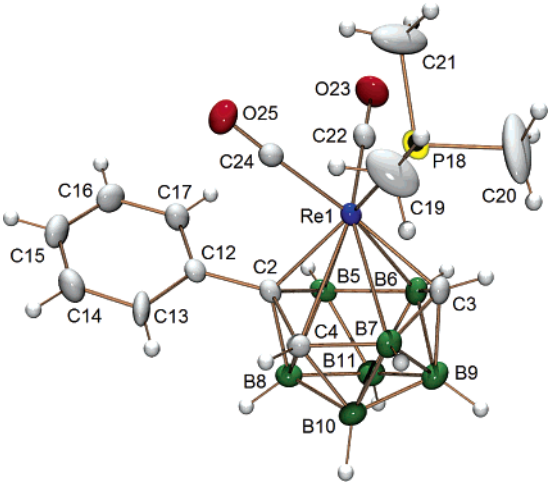

Figure 9. ORTEP representation of the structure of 1,1-$(CO)_2$-1-$P(CH_3)_3$-2-Ph-*closo*-1,2,3,4-$ReC_3B_7H_9$ (**9**). Selected distances (Å) and angles (deg): Re1−C2, 2.162(3); Re1−C3, 2.150(3); Re1−C4, 2.543(3); Re1−B5, 2.402(3); Re1−B6, 2.428(4); Re1−B7, 2.528(4); C2−C12, 1.493(4); C2−C4, 1.517(4); C4−B7, 1.741(4); B7−C3, 1.596(4); C3−B6, 1.587(4); B6−B5, 1.869(5); B5−C2, 1.609(4); Re1−P18, 2.417(1); Re1−C22, 1.873(3); C22−O23, 1.158(4); Re1−C24, 1.939(3); C24−O25, 1.145(4); C2−Re1−C3, 99.3(1); Re1−C2−C12, 123.0(2); C2−Re1−P18, 148.9(1); C2−Re1−C22, 114.7(1); C2−Re1−C24, 84.0(1); C3−Re1−P18, 85.1(1); C3−Re1−C22, 112.8(1); C3−Re1−C24, 157.0(1); Re1−C22−O23, 178.0(3); Re1−C24−O25, 178.3(3).

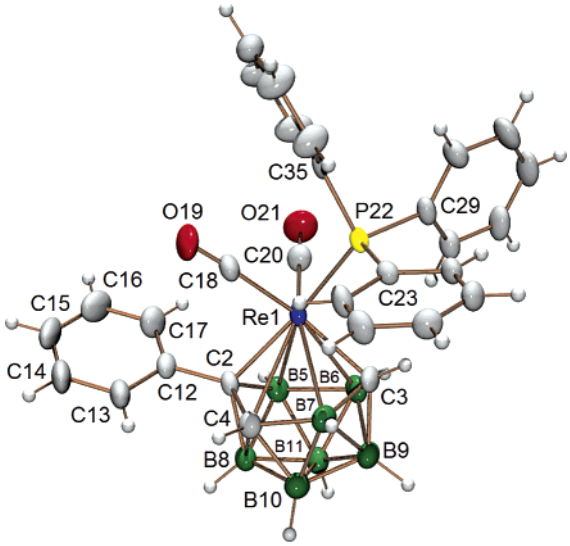

Figure 10. ORTEP representation of the structure of 1,1-$(CO)_2$-1-$P(C_6H_5)_3$-2-Ph-*closo*-1,2,3,4-$ReC_3B_7H_9$ (**10**). Selected distances (Å) and angles (deg): Re1−C2, 2.179(3); Re1−C3, 2.127(3); Re1−C4, 2.628(3); Re1−B5, 2.386(3); Re1−B6, 2.409(3); Re1−B7, 2.565(4); C2−C12, 1.502(4); C2−C4, 1.518(4); C4−B7, 1.737(5); B7−C3, 1.599(5); C3−B6, 1.593(5); B6−B5, 1.872(5); B5−C2, 1.624(4); Re1−C18, 1.957(3); C18−O19, 1.137(4); Re1−C20, 1.872(3); C20−O21, 1.166(4); Re1−P22, 2.417(1); C2−Re1−C3, 98.2(1); Re1−C2−C12, 122.6(2); C2−Re1−C18, 82.4(1); C2−Re1−C20, 106.8(1); C2−Re1−P22, 158.8(1); C3−Re1−C18, 146.6(1); C3−Re1−C20, 122.2(1); C3−Re1−P22, 84.2(1); Re1−C18−O19, 176.9(3); Re1−C20−O21, 177.0(3).

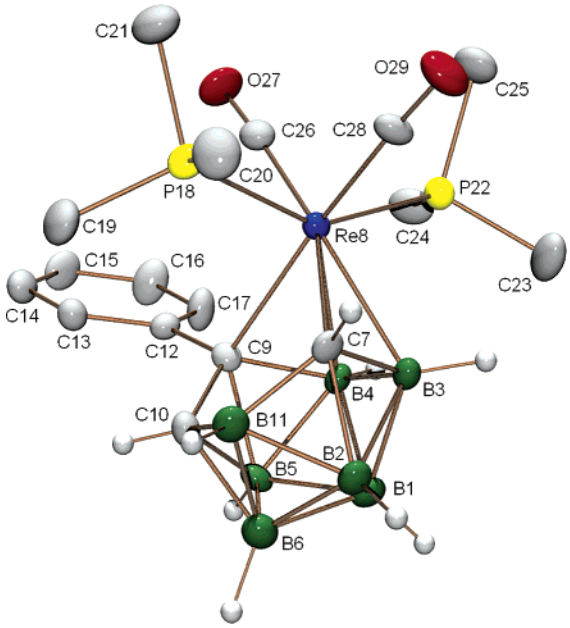

Figure 11. ORTEP representation of the structure of 8,8-$(CO)_2$-8,8-$(P(CH_3)_3)_2$-9-Ph-*nido*-8,7,9,10-$ReC_3B_7H_9$ (**11**) (non-cage hydrogens have been removed for clarity). Selected distances (Å) and angles (deg): Re8−C9, 2.320(3); Re8−C7, 2.288(3); Re8−C10, 3.232(3); Re8−B4, 2.341(3); Re8−B3, 2.357(3); Re8−B11, 3.265(4); C9−C12, 1.522(4); C9−C10, 1.521(4); C10−B11, 1.633(5); B11−C7, 1.608(5); C7−B3, 1.625(5); B3−B4, 1.879(5); B4−C9, 1.648(5); Re8−P18, 2.473(1); Re8−P22, 2.455(1); Re8−C26, 1.942(4); C26−O27, 1.155(4); Re8−C28, 1.922(3); C28−O29, 1.168(4); C9−Re8−C7, 77.7(1); Re8−C9−C12, 114.6(2); C9−Re8−P18, 94.1(1); C9−Re8−P22, 108.8(1); C9−Re8−C26, 91.5(1); C9−Re8−C28, 166.5(1); C7−Re8−P18, 77.9(1); C7−Re8−P22, 124.3(1); C7−Re8−C26, 157.2(1); C7−Re8−C28, 89.0(1); Re8−C26−O27, 176.9(3); Re8−C28−O29, 174.8(3).

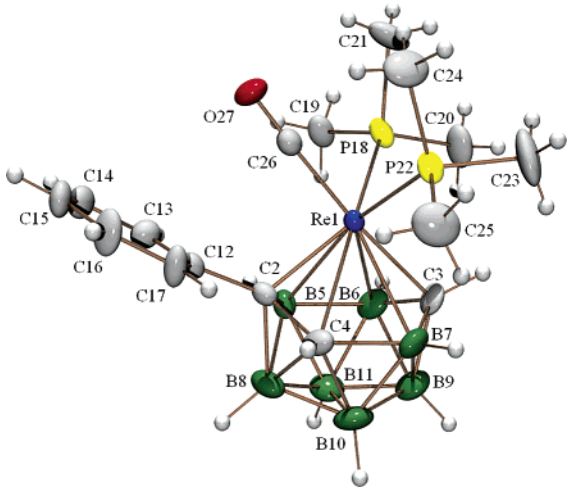

Figure 12. ORTEP representation of the structure of 1-CO-1,1-$(P(CH_3)_3)_2$-2-Ph-*closo*-1,2,3,4-$ReC_3B_7H_9$ (**12**). Although the gross geometry is confirmed, the observed bond distances and angles are not listed because of disorder.

but when the reaction was performed at −78 °C, the solution color immediately changed from red-orange to yellow and a new ^{11}B NMR spectrum was observed that was different than that of either **2** or **7**. This yellow species was stable over a period of days at −78 °C. As can be seen in Figure 13, the ^{11}B NMR spectrum of this intermediate is similar to that of the η^4-coordinated complex, **4** and is thus consistent with the formation of the η^4-coordinated intermediate, 8,8,8-$(CO)_3$-8-$(P(CH_3)_3)$-9-Ph-*nido*-8,7,9,10-$MnC_3B_7H_9$. The ^{11}B NMR spectrum and color did not change, nor was there any gas formation noted as the complex was warmed from −78 to −40 °C (eq 15). However, when the temperature was increased to room temperature, this

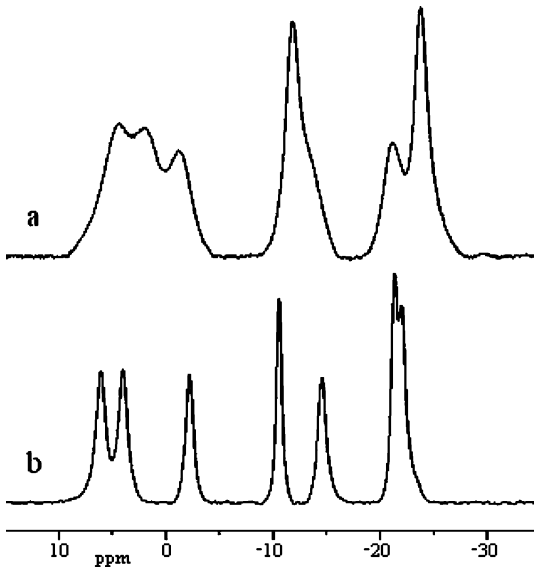

Figure 13. (a) ^{11}B NMR spectrum (taken at −40 °C) of the proposed η^4-coordinated intermediate, 8,8,8-$(CO)_3$-8-$P(CH_3)_3$-9-Ph-*nido*-8,7,9,10-$MnC_3B_7H_9$, initially formed at −78 °C in the reaction of 1,1,1-$(CO)_3$-2-Ph-*closo*-1,2,3,4-$MnC_3B_7H_9$ (**2**) with $P(CH_3)_3$. (b) ^{11}B NMR spectrum of the η^4-coordinated complex 8-($CNBu^t$)-8,8,8-$(CO)_3$-9-Ph-*nido*-8,7,9,10-$MnC_3B_7H_9$ (**4**).

intermediate slowly converted to **7** with evolution of CO (eq 16).

$$1,1,1\text{-}(CO)_3\text{-}2\text{-Ph-}closo\text{-}1,2,3,4\text{-}MnC_3B_7H_9\ (\mathbf{2}) + PMe_3 \xrightarrow{-78\ \text{to}\ -40\ ^\circ\text{C}} 8,8,8\text{-}(CO)_3\text{-}8\text{-}(P(CH_3)_3)\text{-}9\text{-Ph-}nido\text{-}8,7,9,10\text{-}MnC_3B_7H_9 \quad (15)$$

$$8,8,8\text{-}(CO)_3\text{-}8\text{-}(P(CH_3)_3)\text{-}9\text{-Ph-}nido\text{-}8,7,9,10\text{-}MnC_3B_7H_9 \xrightarrow[\text{or } -40^\circ\text{C, 2 h}]{-40\ ^\circ\text{C to rt}} 1,1\text{-}(CO)_2\text{-}1\text{-}(P(CH_3)_3)\text{-}2\text{-Ph-}closo\text{-}1,2,3,4\text{-}MnC_3B_7H_9\ (\mathbf{7}) + CO \quad (16)$$

It was found that, if a solution of 8,8,8-$(CO)_3$-8-$(P(CH_3)_3)$-9-Ph-*nido*-8,7,9,10-$MnC_3B_7H_9$ was maintained at −40 °C, it slowly converted to **7**. This conversion was monitored by recording the ^{11}B NMR spectrum of the reaction mixture every 15 min over a 2 h period (Figure 14). As the reaction proceeded (spectra a−i), it was noted that concurrent with the disappearance of the peaks (▼) representative of the yellow intermediate was the formation of peaks (#) representative of the product, **7**.

Disubstitution Reactions. The disubstitution reactions of (η^5-C_5H_5)$Mn(CO)_3$,[34] (η^5-C_5Me_5)$Re(CO)_3$,[35] and their derivatives have been accomplished by photolysis of the parent complex in the presence of the substituting ligand, but they required much longer reaction times than the monosubstitution reactions.

On the other hand, the reaction of **9** with another equivalent of PMe_3 did not require photolysis but proceeded readily at room temperature to produce the cage-slipped complex **11** (eq 17).

$$1,1\text{-}(CO)_2\text{-}1\text{-}PMe_3\text{-}2\text{-Ph-}closo\text{-}1,2,3,4\text{-}ReC_3B_7H_9\ (\mathbf{9}) + PMe_3 \rightarrow 8,8\text{-}(CO)_2\text{-}8,8\text{-}(P(CH_3)_3)_2\text{-}9\text{-Ph-}nido\text{-}8,7,9,10\text{-}ReC_3B_7H_9\ (\mathbf{11}) \quad (17)$$

The ^{11}B NMR spectrum (Table 1) of **11** is similar to those of **4** and **5**. The ^{1}H NMR spectrum shows, as in **4** and **5**, a lower-field C−H resonance (2.92 ppm) and a higher-field resonance (1.54 ppm) for each hydrogen attached to a cage carbon.

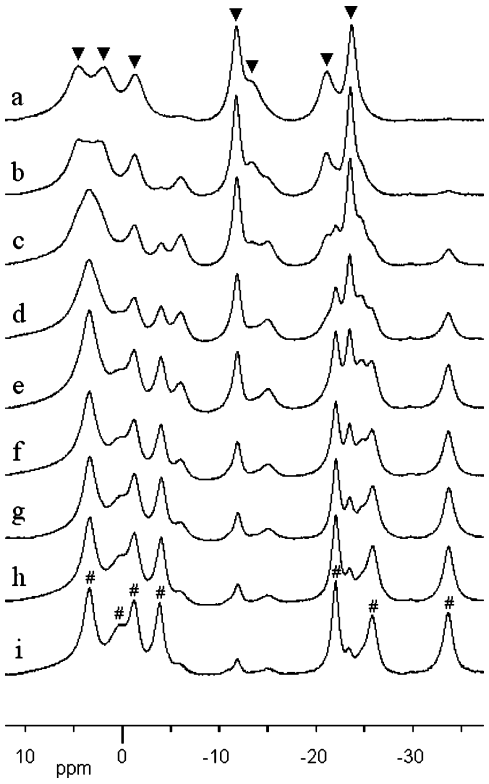

Figure 14. Series of $^{11}B\{^1H\}$ NMR spectra taken every 15 min over 2 h at −40 °C of the reaction of 1,1,1-$(CO)_3$-2-Ph-*closo*-1,2,3,4-$MnC_3B_7H_9$ (**2**) with PMe_3, showing the initial formation of the proposed η^4-coordinated intermediate, 8,8,8-$(CO)_3$-8-$P(CH_3)_3$-9-Ph-*nido*-8,7,9,10-$MnC_3B_7H_9$ (▼), which gradually lost carbon monoxide to produce the final η^6-coordinated product, 1,1-$(CO)_2$-1-$P(CH_3)_3$-2-Ph-*closo*-1,2,3,4-$MnC_3B_7H_9$ (**7**) (#).

11 should be isoelectronic with **4** and **5**, and a crystallographic determination confirmed its predicted *nido* geometry, with the formation of a five-membered, Re8−C7−B11−C10−C9, open face. The metal is again η^4-coordinated to and approximately centered over the C7−B3−B4−C9 face of the tricarbadecaboranyl cage (Figure 11). The Re8−P18 (2.473(1) Å) and Re8−P22 (2.455(1) Å) bond distances in **11** are longer than the Re1−P18 bond distance in **9** (2.417(1) Å) due to the increased electron donation provided by the second $P(CH_3)_3$ ligand. Because of the change in hapticity of the tricarbadecaboranyl cage and the formation of the Re8−C7−B11−C10−C9 open face, the dihedral angle between the C7−Re8−C9 and C9−C10−B11−C7 planes (25.7(2)°) in **11** is much smaller than the equivalent dihedral angle between the C2−Re1−C3 and the C2−C4−B7−C3 planes (59.7(1)°) in **9**. This dihedral angle in **11** is also smaller than the equivalent dihedral angle in the cage-slipped isocyanide complexes **4** (29.4(1)°) and **5** (29.3(3)°). This is likely due to the increased steric requirements of two $P(CH_3)_3$ ligands.

Like **5**, photolysis of **11** with a slight excess of $P(CH_3)_3$ resulted in the loss of CO to form the disubstituted complex **12** (eq 18).

(34) Strohmeier, V. W.; Barbeau, C. *Z. Naturforsh.* **1962**, *17b*, 848−849.
(35) Bergman, R. G.; Seidler, P. F.; Wenzel, T. T. *J. Am. Chem. Soc.* **1985**, *107*, 4358−4359.

$$8,8\text{-}(CO)_2\text{-}8,8\text{-}(P(CH_3)_3)_2\text{-}9\text{-Ph-}nido\text{-}8,7,9,10\text{-}ReC_3B_7H_9\ (\mathbf{11}) \xrightarrow{h\nu} 1\text{-CO-}1,1\text{-}(P(CH_3)_3)_2\text{-}2\text{-Ph-}closo\text{-}1,2,3,4\text{-}ReC_3B_7H_9\ (\mathbf{12}) + CO \quad (18)$$

The ^{11}B NMR spectrum (Table 1) of **12** is similar to that of **3**. The ^1H NMR spectrum shows, as in **3**, a higher-field C−H resonance for the proton attached to C4 (1.50 ppm) and a lower-field C−H resonance for the proton attached to C3 (3.69 ppm). The resonances for the protons attached to C3 and C4 shift upfield on going from **3** (6.29 and 2.60 ppm) to **9** (5.06 and 2.06 ppm) and **12** (3.68 and 1.54 ppm), thus indicating an increase in electron donation to the metal and cage system as CO is replaced with $P(CH_3)_3$.

12 should be isoelectronic with **3**, and a crystallographic determination confirmed its predicted *closo* geometry (Figure 12). Unfortunately, disorder in the crystal structure prevents any detailed analysis of bond lengths and angles.

Conclusions

A possible associative mechanism for the carbonyl substitution reactions of $1,1,1\text{-}(CO)_3\text{-}2\text{-Ph-}closo\text{-}1,2,3,4\text{-}MC_3B_7H_9$ [M = Mn (**2**) and Re (**3**)], that is consistent with the results of the crystallographic and spectroscopic studies reported herein, is given in Figure 15a. As evidenced by both the isolation of $8\text{-}(CNBu^t)\text{-}8,8,8\text{-}(CO)_3\text{-}9\text{-Ph-}nido\text{-}8,7,9,10\text{-}MC_3B_7H_9$ [M = Mn (**4**), Re (**5**)] and the observance of an $8,8,8\text{-}(CO)_3\text{-}8\text{-}(P(CH_3)_3)\text{-}9\text{-Ph-}nido\text{-}8,7,9,10\text{-}MnC_3B_7H_9$ intermediate species in the NMR studies of the PMe_3 substitution reaction of **2**, the incoming ligands attack at the metals before dissociation of a carbonyl group. To maintain the 18-electron count of the resulting complexes, the tricarbadecaboranyl ligand reduces its electron donation to the metal from six to four electrons by the $\eta^6-\eta^4$ cage-slippage. Following carbonyl dissociation, the cage then undergoes an $\eta^4-\eta^6$ coordination change with a concurrent increase in electron donation to the metal center from four to six electrons, thereby restoring the 18-electron count of the metal in the new monosubstituted dicarbonyl complexes. Because of the additional steric crowding, an associative reaction mechanism should be less likely to be involved in the formation of disubstituted complexes, such as $1\text{-CO-}1,1\text{-}(P(CH_3)_3)_2\text{-}2\text{-Ph-}closo\text{-}1,2,3,4\text{-}ReC_3B_7H_9$ (**12**), but even here the isolation of the cage-slipped complex $8,8\text{-}(CO)_2\text{-}8,8\text{-}(P(CH_3)_3)_2\text{-}9\text{-Ph-}nido\text{-}8,7,9,10\text{-}ReC_3B_7H_9$ (**11**) and its subsequent conversion to **12** confirms an associative reaction pathway (Figure 15b).

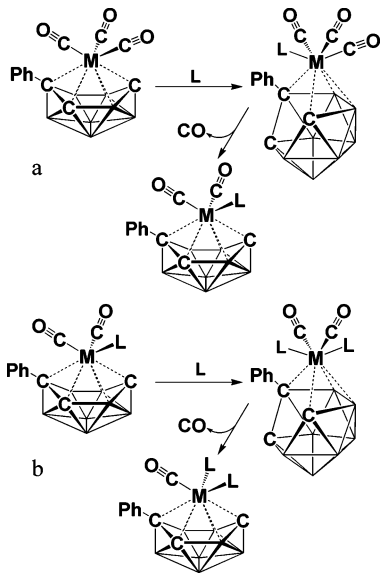

Figure 15. Proposed associative mechanism for the (a) mono- and (b) dicarbonyl substitution reactions of $1,1,1\text{-}(CO)_3\text{-}2\text{-Ph-}closo\text{-}1,2,3,4\text{-}MC_3B_7H_9$ [M = Mn, Re] with $CNBu^t$ and PR_3 (R = Me, Ph) via cage-slipped η^4-intermediates.

Other recent studies of **2** and **3** have shown that both Mn and Re readily undergo one- and two-electron electrochemical and chemical reductions that are also facilitated by the $\eta^6-\eta^4$ cage-slippage. The fact that one-electron reduction potentials for **2** and **3** are each ~1.9 V more positive of those of $(\eta^5\text{-}C_5H_5)M(CO)_3$ [M = Mn, Re] again illustrates that the cage-slippage is dramatically more favorable than the $\eta^5-\eta^3$ ring-slippage of their cyclopentadienyl counterparts.[36] The ability to readily open a vacant coordination site at the metal by such a facile cage-slippage process may prove to be valuable in many potential catalytic reactions of tricarbadecaboranyl metal carbonyl complexes. We are now exploring these possibilities.

Acknowledgment. The National Science Foundation is gratefully acknowledged for their support of this research.

Supporting Information Available: X-ray crystallographic data for structure determinations of **2**−**12** (CIF). This material is available free of charge via the Internet at http://pubs.acs.org.

JA062201U

(36) Nafady, A.; Geiger, W. E.; Butterick, R.; Carroll, P. J.; Sneddon, L. G., unpublished results.